Charles University in Prague
Faculty of Mathematics and Physics

Diploma Thesis

Ondřej Chvála

Extraction of Inclusive Cross Sections of Charged Pions Produced in Proton–Proton Collisions from the NA49 Experiment Data

Institute of Particle and Nuclear Physics

Supervisor of diploma thesis: Prof. Hans Gerhard Fischer
Consultant of diploma thesis: Dr. Jiří Dolejší

Study programme: Nuclear and Sub-nuclear Physics

I would like to thank everyone, without whom this thesis could not be written. Especially my supervisor Prof. H. G. Fischer for providing me the possibility work in CERN, for introducing me into the subject, for giving me of the literature, and last but not least for the advice; my consultant Dr. Jiří Dolejší for his advice and patience with my work and the members of NA49 collaboration for the pleasant and helpful atmosphere.

I confess I have written my diploma thesis on my own,using only quoted sources. I agree with lending of the thesis

Prague, April 21, 2000. Ondřej Chvála

Contents

1 Introduction **1**

2 The NA49 Experiment **3**
2.1 Overview . . . 3
2.2 NA49 Detector . . . 4
2.2.1 The SPS Accelerator . . . 4
2.2.2 Beam Particles and Targets . . . 4
2.2.3 Beam Definition and Triggers . . . 5
2.2.4 The Magnets . . . 6
2.2.5 The Time Projection Chambers . . . 6
2.2.6 The Time of Flight Detectors . . . 7
2.2.7 The Calorimeters . . . 8
2.2.8 Veto Proportional Plates . . . 9
2.2.9 Centrality detector . . . 9
2.3 Data Acquisition . . . 9
2.3.1 NA49 electronics . . . 10
2.4 Event Reconstruction . . . 10
2.4.1 Cluster Finding . . . 11
2.4.2 Tracking . . . 11
2.4.3 V0 Finding . . . 11
2.4.4 Primary vertex resolution . . . 12
2.4.5 The dE/dx Calibration . . . 12
2.5 NA49 Data standards . . . 12
2.5.1 DST and DS PACK . . . 12
2.5.2 μDST . . . 12

3 Extracting of the Inclusive Cross Sections **14**
3.1 Hadronic cross sections . . . 14
3.2 Measuring of the reaction cross section . . . 15
3.2.1 Trigger cross section σ_{tr} . . . 15
3.2.2 Inclusive cross section σ_{inc} . . . 16
3.3 Gas Ionization by Charged Particles . . . 16
3.3.1 Energy loss dE/dx . . . 16

3.3.2 Truncated mean . . . 17
3.4 Data binning . . . 18
3.4.1 Manual binning . . . 18
3.4.2 Binning algorithms . . . 18
3.5 Data cuts . . . 18
3.6 dE/dx fit method . . . 19
3.6.1 Fit quality . . . 21
3.6.2 MC simulation of dE/dx . . . 21
3.7 Corrections . . . 22
3.7.1 Bethe-Bloch shifts and σ_{rel} . . . 22
3.7.2 Weight factors and σ_{vertex} . . . 23
3.7.3 Acceptance . . . 23
3.7.4 Feed over . . . 23

4 Description of Algorithms 25
4.1 Development remarks . . . 25
4.2 Technique Used . . . 27
4.2.1 Binning . . . 27
4.2.2 Data cuts . . . 29
4.2.3 MC simulation and fitting . . . 29
4.2.4 Extracting the results from bin directories . . . 31
4.2.5 Fitting IIC surface . . . 31
4.2.6 Interpolating IIC values . . . 33
4.2.7 Binning comparison and Acceptance check . . . 34
4.3 Comparison with models . . . 35

5 Results 36
5.1 Extracted data . . . 36
5.1.1 Fit parameter tables - positive tracks . . . 37
5.1.2 Fit parameter tables - negative tracks . . . 38
5.1.3 Discussion . . . 39
5.1.4 Binning C . . . 39
5.2 Comparison with the data in literature . . . 42
5.3 Comparison with Event Generators . . . 45
5.3.1 Manually defined bins . . . 45
5.3.2 Automated binning . . . 45
5.4 Experience with corrections . . . 47
5.4.1 Shifts and σ_{rel} . . . 47
5.4.2 φ distribution of tracks . . . 48

6 Conclusions 49

A Kinematic Variables 53

B Data Measured by NA49 **55**

C The μDST **56**
C.1 Data Structure 56
C.2 Parameterization of the Bethe-Bloch curve 58

D Source Codes of Mentioned Programmes **59**

Abstract

The aim of my diploma work is to develop the method of automated extraction of the inclusive cross sections of charged pions produced in proton–proton interactions at $\sqrt{s} = 17.3\,\mathrm{GeV}$ from NA49 data by means of fitting simulated dE/dx histograms to the measured one (so called *"dE/dx fit method"*) and test it on present data set.

Chapter 1

Introduction

Experiment NA49 was built-up in order to study central Pb-Pb collisions at SPS accelerator and with the primary aim to discover the deconfined state of hadronic matter, the so-called Quark-Gluon Plasma (QGP). According to [26] and the recent CERN seminar devoted to experimental results of CERN's Lead-Beam Programme [27], several traces of QGP formation have been measured, and so, this basic intention has been satisfied.

However, NA49 detector is an ideal device with large acceptance, excellent momentum resolution, good particle identification (PID) and the ability to record many events per beam spill. Thus, it is also a great tool to study less ambitious but highly desirable properties of elementary nucleon–nucleon and nucleon–nuclei interactions with controlled centrality.

NA49 collaboration has been collecting the extensive and unique set of data on different hadronic collision processes since 1994, see Appendix B for complete list. The amount of recorded events, together with large phase space coverage of the detector, allows semi-inclusive analysis.

Even though there were many experiments measuring properties of the soft hadronic interactions – mostly on ISR in early seventies – there is no satisfactory theory of these interactions. This is because of well-known difficulties with treating the nonperturbative regime of QCD. The summary of already measured low p_T inclusive spectra can be found in [6].

This theoretical fecklessness makes precise experimental research in this field very indigent and useful for several reasons. For example, deciding among phenomenological models of soft hadron interactions, which has been impossible in the past[10]; and the fine-tuning of the parameters of event generators like Fritiof or Nexus to better describe the interactions, which then allows better background estimation for more spectacular processes.

However, some members of the NA49 collaboration are convinced that the detailed analysis of our large set of p-p, p-A and A-A data can reveal some more fundamental understanding of soft hadronic interactions, rather than just the re-tuning of model parameters.

This belief is supported by the first semi-inclusive look at this data, which showed astonishing (maybe not so astonishing for people working in the field for a longer period) results: a simple-minded model with the assumption of independent nucleon-nucleon collisions explains most of the phenomena observed at central Pb-Pb collisions as well as QGP collective models do [25]. Doubts about clear evidence of QGP formation at the SPS energy was admitted even by several speakers at [27][1], and a need for detailed understanding of p-p, p-A and A-A interactions was also expressed.

The problem of NA49 has been an unreliable reconstruction chain[2] so far. The priority of the second half of 1999 and of the beginning of 2000 has been debugging and tuning of the reconstruction chain to satisfactory functionality and the reconstruction of all the measured raw data in one go. This will provide comparable and reliable data sets, which should be completed in summer 2000.

Detailed semi-inclusive studies of newly reconstructed data and prospective new measurements ought to be the main research programme of the NA49 collaboration in a near future.

My contribution to the NA49 collaboration consists from developing a dE/dx fit method, applying it to existing data from 1996 processed by the old reconstruction chain, to obtain the invariant inclusive cross sections of charged pion production, and compare the results with existing data and event generators. My programs can also be used to check the new reconstruction chain.

[1] U. Heinz: "There is no question that these exciting observations constitute a quantum jump in our understanding of matter at extremely high temperatures and densities and testify to the great success of the CERN heavy ion program. In spite of the above, the evidence is not enough to prove, beyond reasonable doubt, the creation of Quark-Gluon Plasma."

[2] Reconstruction chain is a set of programs which extracts physical information about event from the raw data. This includes a cluster finding, tracking, track's momentum fitting, looking for decays of neutral strange particles like K or Λ (so called V0-fitting), main interaction vertex fitting and dE/dx calibration. This subject is deeply discussed in the section 2.4, page 10

Chapter 2

The NA49 Experiment

This chapter provides a short look at the scope of the NA49 experiment.

2.1 Overview

The NA49 detector was built-up with the intention of studying hadron production off relativistic heavy ion collisions following the NA35 experiment. This experiment was investigating collisions of intermediate mass ions like sulphur or carbon by means of the streamer chambers. Detector itself is located on the same place as its forerunner on the H2 line of the North experimental hall of the SPS accelerator in the Prevessin part of the CERN.

The NA49 was designed to study complex central Pb-Pb events with up to 10^3 produced charged hadrons per event on an event-by-event basis. It was necessary to use a large acceptance detector with precise tracking, good track resolution and particle identification for this purpose.

These requirements have been fulfilled by means of four Time Projection Chambers (TPCs) as a primary charged particle tracking detector, several Time of Flights walls, calorimeters, proportional chambers, scintillation counters and other sub-detectors, for the detector diagram see picture 2.1.

Due to the fixed-target geometry, particles produced from the collision at the SPS energy are emitted in a very narrow cone along the beam because of the large momentum of the center-of-mass system. This requires a strong and homogeneous magnetic field to spread the charged particles apart and to provide the momentum measurement through the curvature of the particle track in the field.

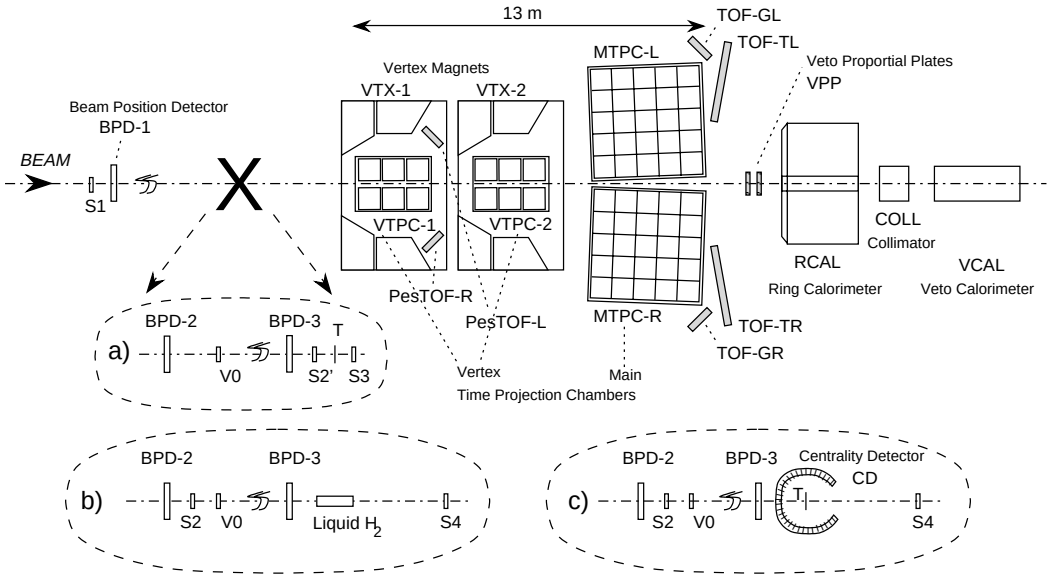

Figure 2.1: Schema of the NA49 experimental layout, including different reaction configurations: a) A-A, b) p-p, c) p-A. The picture has been taken from [1] and modified.

2.2 NA49 Detector

2.2.1 The SPS Accelerator

The protons or lead ions used in NA49 are produced by linear accelerators. They are injected into the Proton Synchrotron Booster where they are accelerated to 95 A.MeV/c, then passed into the Proton Synchrotron (PS) and accelerated to 4.5 A.GeV/c. Final acceleration is done in the SPS circle, which is able to accelerate protons to laboratory momenta of 450 GeV/c, intermediate mass ions up to 200 GeV/c per nucleon and Pb ions up to 158 GeV/c per nucleon. The particles are delivered in short and separate spills.

2.2.2 Beam Particles and Targets

NA49 uses two types of targets, either a solid – wafer of Pb, Si, Al, C, ..., or a vessel with liquid hydrogen.

Beam particles can be extracted either directly from the SPS, or secondary beams can be formed from the products of an interaction of the beam with the fragmentation target – pions, kaons, protons, deuterons and large nuclei up to Phosphorus. The fragmentation target is placed about 30 m before the experimental one and the material used is 1 cm of carbon.

Picture 2.2 shows the fragment spectra starting from Boron.

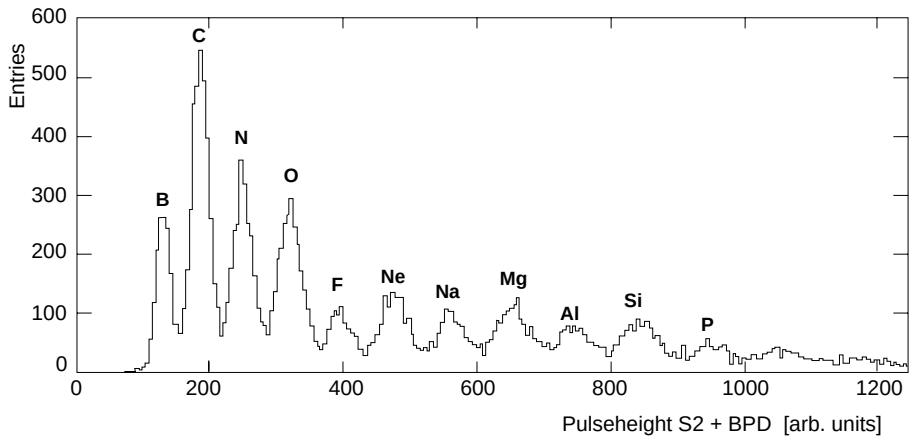

Figure 2.2: Fragmentation beam composition, fragments lighter than boron not shown, taken from [1].

This versatile experimental setup allows the examination of various types of hadron interactions.

2.2.3 Beam Definition and Triggers

The position of incoming beam particles is measured by three Beam Position Detectors (BPD $1, 2, 3$) with the precision of a few hundred μm. Their signals can be also used to select proper fragments from the fragmentation beam by means of dE/dx.

BPDs are small ($3 \times 3\,\mathrm{cm}^2$) proportional wire chambers with two orthogonal cathode strip readouts. They are filled with a Ar/CH_4 80/20 gas mixture.

A variety of detectors is used to determine the beam trigger: two Čerenkov counters, S1 and S2, upstream from the target; scintillation counters, V0 and V1, with a 1 cm hole in the center, also upstream from the target; S4 counter downstream from the target; and a scintillation counter, T0, to start an event timing.

The beam is defined by a coincidence between S1 and S2 together with anti-coincidence of V0 and V1. A signal in V0 or V1 indicates an interaction before the target, either with air or with material from the detectors upstream.

The beam signal together with no signal in S4 means that a valid beam particle has passed the target, but that track did not continue after the target, indicating that some interesting interaction occurred. This causes a trigger, i.e., the detector electronics read out the information about such an event.

Each type of interaction requires slightly different trigger conditions. For Pb runs, also the calorimeters signals are used for triggering.

2.2.4 The Magnets

There are two super-conducting Helmholtz-arranged magnets placed directly behind the target, the first with a field of 1.5 T and the second of 1.1 T.

This field allows for the determination of the momentum of particles which left the tracks in the detectors placed inside the magnets and also draws apart different particle tracks for better track separation.

Magnets are cooled by liquid helium.

2.2.5 The Time Projection Chambers

The Time Projection Chamber (TPC) is the most sophisticated current detector employing gas ionization; it provides three-dimensional tracking ability and particle identification (PID) over a large volume.

NA49 uses four TPCs, two "vertex TPC" (VTPC1, VTPC2) placed within the magnets, and two large "main TPC" (MTPCL, MTPCR) on either side of the beam line further downstream.

The TPC consists of a large gas-filled sensitive volume, a multi-wire proportional section and a readout pad plane. The **sensitive volume** is surrounded by an electric field cage, which provides a constant drift velocity for electrons from ionization. On the top of the TPC there are several **wire planes**, which provide multiplication of the charge of incoming electrons and gating. The **pad plane** consists of many small pads of various sizes, depending on the desired spatial resolution (according to expected track densities), where the charge is collected and read out.

When a charged particle travels through the TPC volume, it ionizes gas molecules along its path. Created electrons travel in the drift field upwards to the multi-wire region. In this region electrons are rapidly accelerated towards the high-voltage sense-wire plane causing an avalanche of electrons onto the wire – the charge multiplication. Meanwhile, a mirror charge from the ions created by this ionization is generated on the pad plane. This pad signal is read out. The gating grid encages these ions in the multi-wire section after the avalanche, preventing them from drifting to the sensitive volume and reducing the signal by recombination, see drawing 2.3.

NA49 uses an innovative design for the field cage: because of the large size of the chambers, a field cage made from copper strips would be too heavy. A much lighter cage is constructed from aluminized Mylar strips suspended on ceramic rods placed vertically in the cage corners, see picture 2.4. This design also decreases the probability of the secondary interactions of measured particles with the field cage itself.

There are different gases used in VTPCs and MTPCs. MTPCs are filled up with the following gas mixture: 91 % Ar / 4.5 % CH_4 / 4.5 % CO_2 , VTPCs uses 91 % Ne / 9 % CO_2, which produces less diffusion resulting in better two-track resolution.

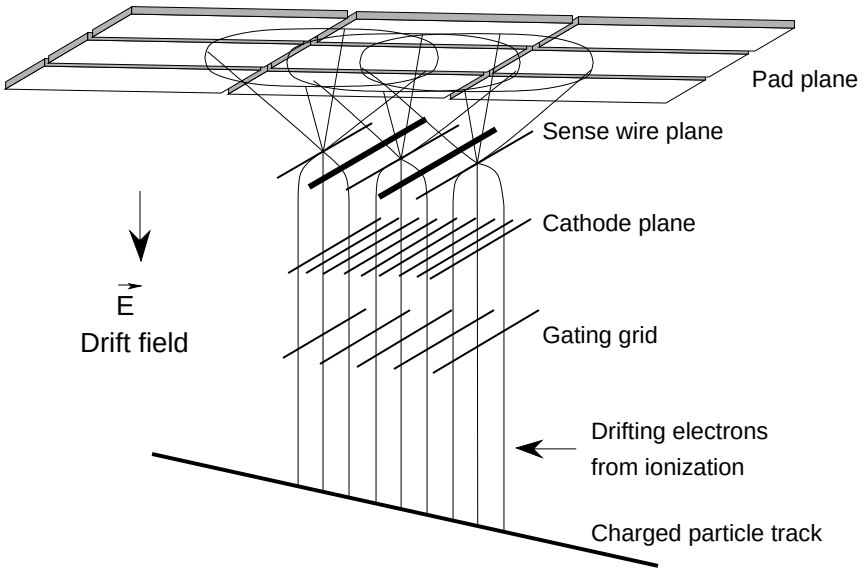

Figure 2.3: Schematic layout of the TPC readout section, taken from [1].

A summary of the parameters of the TPCs used is shown in table 2.1. Upper values of MTPC's pad size are valid for the high-resolution sectors of the chamber, the lower for the standard ones.

Momentum resolution $\Delta p/p^2$ of the TPCs varies from 7×10^{-4} $(\mathrm{GeV/c})^{-1}$ for tracks passing through VTPC1 only, to 3×10^{-5} $(\mathrm{GeV/c})^{-1}$ for so-called global tracks detected in VTPCs and one MTPC.

2.2.6 The Time of Flight Detectors

NA49 uses several Time of Flight (TOF) detector systems. They serve to improve PID in momentum regions where dE/dx information from TPCs is useless due to overlapping of the particle's dE/dx.

	VTPC	**MTPC**
Size [cm]	260 × 200 × 72	384 × 384 × 129
No. of pads	27 648	63 360
Pad size [mm]	3 × 28	3.13 × 39
		4.95 × 39
Drift length [cm]	66.6	111.7
Drift velocity [cm/μs]	1.4	2.4
Drift field [V/cm]	200	175
Drift voltage [kV]	13	16.5

Table 2.1: NA49 TPCs parameters

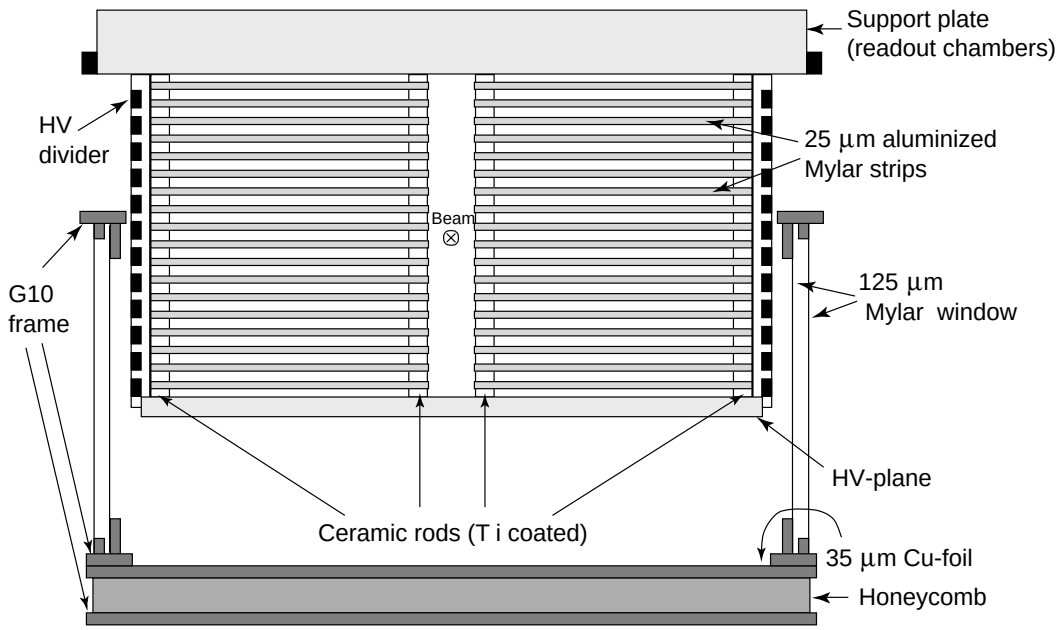

Figure 2.4: Schematic picture of a VTPC assembly, taken from [1].

There are two pixel scintillating walls (TOF-TL and TOF-TR in figure 2.1), each one with 1782 pairs of rectangular scintillator and photo-multiplier, with a 60 ps time resolution.

Detector walls TOF-GL and TOF-GR are designed differently. These walls are made of two plates of horizontally and vertically oriented scintillating rods, each of them with photo-multipliers at both ends. Time resolution of this detector has been determined to be 85 ps.

PesTOF[1] detectors are small-gap spark counters. They are devised to improve NA49 PID in the backward hemisphere. Their time resolution is estimated to be below 50 ps. So far, one array was installed mostly for test and development purposes.

2.2.7 The Calorimeters

The NA49 experiment is equipped with two calorimeters – the Ring Calorimeter (RCal) and the Veto Calorimeter (VCal). Both of them have an electromagnetic and a hadronic section. They have been used in many CERN experiments, starting with NA5.

RCal is used to measure transversal energy in heavy ion collisions. The detector is placed symmetrically around the beam, which flies through the hole in the middle of the RCal.

[1]Pestov TOF

In nucleon–nucleon runs the detector is shifted transversely to the beam axis so its active volume is placed behind the gap between the MTPCs in order to measure particles emitted in the very forward direction. Its data will be used for measuring leading baryon energy and – together with VPP – to decide if this baryon is a proton or a neutron. Combined information from tracking in TPCs, RCal and VPP allows for distinguishing pions from electrons with high momentum ($p \gtrapprox 50\,\mathrm{GeV}$).

The signal from VCal is used as a trigger in heavy ion runs for selecting the event's centrality. For this purpose there is an iron collimator (Coll) in front of the VCal.

2.2.8 Veto Proportional Plates

The Veto Proportional Plates (VPP) were constructed in summer 1999 to "close" the NA49 acceptance gap in the very forward region where there is no acceptance provided by TPC – the inter-space between MPTCs and a 20 cm wide blind region in the center of VTPCs. These gaps are necessary in ion runs, because of the extreme ionization of the lead beam and its fragments, which would distort the uniformity of a drift field in a TPC. In QGP research the interest is focused mainly to transversal phenomena, so the acceptance loss is not very painful.

However, in the nucleon–nucleon case, we do not have problems of extremely ionizing nuclei from interactions[2], and the question of the fate of the incoming baryon is for our understanding essential.

VPP are two plate proportional chambers with a cathode strip readout. Each plate has two crossed strip layers. They are placed subsequently between the MTPC gap and the RCal.

2.2.9 Centrality detector

The Centrality Detector (CD) is an unique device developed by NA49 to measure the impact parameter in p-A collisions. The CD surrounds the target and detects slow *"grey"*[3] protons which have been knocked out of the nuclei when the proton came through the nuclei. Detailed description of the CD is in [1], page 6.

This detector is also used for the trigger in p-A runs.

2.3 Data Acquisition

The SPS delivers accelerated particles in spills of five seconds long every twenty seconds. During the spill, the detector is taking data and the elec-

[2]This was tested in a deuteron–proton collisions in 1999 run period. The fragmentation beam with energy of 40 GeV per nucleon went through the MTPCL.

[3]The terminology comes from emulsions.

tronics store it in temporary buffers. Within the fifteen seconds pause between the spills, the data are flushed out to tape or to the Central Data Recording (CDR) storage system of CERN.

2.3.1 NA49 electronics

NA49 readout electronics are placed aside from the detector in the counting hall. The readout is compounded from many CAMACS modules, VME crates and a variety of computers connected together. Experimental electronics are located in about 30 standard 19" racks.

For each detector, there are some crates occupied by corresponding readout modules, all the information is collected in the VME master crate. This crate contains a module with a master processor[4] that builds the event and writes it either to the 100 GB SONY tape or CDR. The tape is used most often, because of its high transfer rate 16 MB/s. Detailed description of the design of NA49 readout system can be found in [2].

Data from the TPCs represents by far the most of the data collected by all of the experiment. The size of one event raw data size can be estimated: 182 016 pads $\times$ 512 time slices $\times$ 1 byte = 89 MB. Even after zero suppression and compression, typical raw event size is about 8.5 MB in the case of central Pb-Pb collisions. [3]

Raw data are stored in the CERN's tape library.

2.4 Event Reconstruction

Events written in raw format have to be reconstructed to a form usable for physical analysis. This task is performed by a huge software collection called the **reconstruction chain** (RC). Performance and reliability of the RC is critical for the plausibility of NA49 results and also for justification of the collaborators work.

Unfortunately, the old reconstruction chain used to process all the data now available is known to have bugs, so the collaboration has been spending much work on improving the RC performance in many ways. During this business, a method of manual eye-scanning of events, proved to be competent and assisted in the correction of many tricky errors.

This effort should lead to a robust RC, which would process all the data recorded in one go to simplify comparison of the results obtained on different data sets. Recently the reconstruction chain have been tested and already some test events are being reconstructed, data reconstructed by a production version are expected in summer 2000.

As most of the information about an event is recorded in TPCs data, only TPCs are considered in the following.

[4] equipped by Motorola 68040 CPU

2.4.1 Cluster Finding

Raw TPC data can be visualized in a three-dimensional space of [padrow[5], pad, time] coordinates. Each element of this array contains integrated charge deposits from ADC readout electronics. The charge created by ionization across a padrow spatially diffuses as it travels up to the readout section. This causes the information about the ionization created somewhere inside the active TPC volume to spread across several pads and time-slices, forming a *charge cluster*.

The cluster finder is a basic part of the reconstruction chain, which searches for the clusters by grouping the information from nearby pads and time-slices within a padrow. The position of each cluster is determined as a center-of-gravity of the charge distribution. The cluster finder also calculates the dE/dx information as a sum of all the pads forming the cluster and corresponding time-slices, i.e. the total charge of the cluster.

The clusters are then used as points which form the tracks.

2.4.2 Tracking

The track finder is a multi-phase algorithm that connects the points within one TPC into track pieces.

With exact knowledge of the TPC's position[6] and the drift velocity, we can interconnect the track pieces in different TPCs to one *global track*. If there are parts of the global track in some of the VTPCs, the momentum and the charge of the particle is measured and assigned to the track.

Global tracking also helps to reduce junk tracks from secondary interactions between the particles and material of the detector, event-corelated particles like muons accompanying the beam or the cosmic rays.

2.4.3 V0 Finding

Some of the tracks come from the primary interaction vertex in the target, some are traces of the strange neutral[7] particles decays, mainly Λs, K^0s, ... or a photon conversion. V0 finder is devised to discover such tracks, calculate the secondary vertex position and assign V0 decay tracks to the secondary vertex.

After identifying decay tracks, re-fitting of the primary vertex follows. Therefore, elimination of these tracks from the primary vertex ones increases the primary vertex resolution.

[5]The padrow is a line of readout pads arranged perpendicularly to the beam direction. There are 72 padrows in a VTPC and 90 in a MTPC.

[6]NA49 TPC's locating is measured by optical methods with absolute precision better than 200 μm.

[7]The decay of a charged particle causes a kink of the track, which can be easily detected by tracking routine

2.4.4 Primary vertex resolution

The position of the primary interaction vertex is evaluated from the vertex track fit. The z axis can be fixed by information from BPDs.

The dependence of primary vertex resolution on the event track multiplicity is much more important in p-p interactions due to the target construction (see section 3.7.2 on page 23) and due to ordinarily lower multiplicity of events than in central Pb-Pb.

2.4.5 The dE/dx Calibration

For the calibration of the gas gain and electronics, the standard method of Kr^{83} gas is used.

This method consists of injecting unstable isomeric Kr^{83} [8] into a TPC volume. This isotope cascades down to its ground state, producing a characteristic spectrum of charge deposition. More details can be found in [1].

Detailed analysis of the Kr^{83} spectra serves also for identification and elimination of bad ADC chips in the readout electronics.

2.5 NA49 Data standards

2.5.1 DST and DS PACK

NA49 data sets are stored in an object-oriented client-server data manager named DS PACK. There is information about all the tracks in events, their points and also secondary vertices found by V0 finder; information from all the non-TPC detectors is also stored in these DSTs[9].

Details about DS PACK and relevant object definitions can be found in [3] and [4].

The DST itself is not suitable for all the kinds of physical analysis, because it contains too much data to work with.

2.5.2 μDST

μDST data format is suitable in such cases, when we are interested only in the primary vertex tracks from the global tracking, as in our case. Data in this format has been created by *Gabor Veres*.

Each μDST is an ASCII file that contains event-by-event information about reconstructed tracks: vertex momentum, charge, measured dE/dx losses and appropriate relative variance $\sigma_{exp}^{dE/dx}$ and some other quantities, which are not needed for our kind of analysis.

[8] half life 1.9 hr, excitation energy 41.6 keV

[9] Data Summary Tapes

In section 3.6.2 on page 21 the origin of dE/dx information in μDST is explained.

Detailed structure of the μDST is described in Appendix C.

Chapter 3

Extracting of the Inclusive Cross Sections

The *cross section* σ is the basic quantity for describing any particle interactions. It corresponds to the effective target area seen by ingoing particles. In another words, it measures the probability of an interaction.

This chapter describes theoretical considerations about extracting the cross sections from NA49 data.

3.1 Hadronic cross sections

Hadronic interactions are specific by very complicated many-particle final states. Because of this complexity, the first studies concerned with the *total cross section* σ_{tot} summed over all possible reaction channels and depended only on one variable, s – the square of the total CMS energy.

The magnitude of the total cross section reflects to some extent the size of the interaction objects. The fact that the hadronic total cross sections are of the order of tens of mb leads us to think of hadrons as objects with the characteristic dimension of a fermi. [8]

The next more complicated object of study are reactions $A + B \to C +$ *anything*, commonly named *one particle inclusive processes*. The invariant cross section of such a type of interaction is defined by:

$$\sigma_{AB}^{C} = E_C \frac{d^3\sigma}{dp_C^3}$$

where $d^3\sigma/dp_C^3$ is the differential cross section, i.e. the probability per unit incident flux, for detecting particle C within the phase-space volume element dp_C^3; E_C is included to ensure the Lorentz invariance of the quantity. [9]

The invariant cross section can be expressed by different formulae depending on a choice of kinematic variables, see Appendix A for their definition. In our case, the cross section is a function of two independent variables

only, because of the φ–symetry of the collisions (the beam is unpolarised).

$$E_C \frac{d^3\sigma}{dp_C^3} = \frac{E_C^{lab}}{\pi} \frac{d^3\sigma}{dp_L^{lab} dp_T^2} = \frac{E_C^{lab}}{p_T p_L^{lab}} \frac{d^3\sigma}{d\varphi dx_F dp_T} = \frac{1}{p_T} \frac{d^3\sigma}{d\varphi dy dp_T} \tag{3.1}$$

The different forms are obtained with the appropriate Jacobian, see [11], [19]. In my programmes the cross sections are calculated as a function of $[x_F, p_T]$ and $[y, p_T]$.[1]

The inclusive cross section for some kind of particles reveals the general or average properties of the particle production in some kind of collision.

A further step in the analysis of hadron interactions consists of several particle inclusive distributions and correlation studies. This kind of approach requires more extensive statistics of events. Thus, it is a challenge for NA49 collaboration, as its data sets will be (after the reconstruction) the world's largest one.

Deeper insight into the scope of soft-hadronic inclusive reactions is provided in [16], [7], [8] or [11]. The fact that most of the mentioned publications come from the late seventies reflects the lack of theoretical and experimental improvement in the field of soft-hadronic physics.

In the following I would like to describe how we can extract invariant inclusive cross sections from NA49 data by means of the specific energy losses dE/dx of charged particles.

3.2 Measuring of the reaction cross section

The general formula for the specific reaction cross section in the fixed target experiment is:

$$\sigma_{int} = \frac{1}{\rho \; l \; N_A/A} \; \frac{N_{int}}{N_{beam}} \tag{3.2}$$

where ρ is the density of the target, l is its length, N_A is the Avogadro number, A is atomic weight of the target material, N_{int} is the number of interactions of a given type, N_{beam} is the number of beam particles that have traversed through the target during the measurement. For detailed discussion see [22].

3.2.1 Trigger cross section σ_{tr}

Trigger cross section is a total cross section of all the interactions the data acquisition electronics trigger.

There are two scintillation counters, S2 and S4, used as a trigger for proton-proton collisions, working in anti-coincidence. S2 is placed in front

[1] As the μDST processed is preliminary, values of the cross sections are presented and discussed only in the $[x_F, p_T]$ coordinate system.

of the target and monitors the beam. S4 detects protons penetrating the target without interaction; for details see [1], page 6.

The value of the trigger cross section can be determined as shown in [22], $\sigma_{tr} = 28.9\,\mathrm{mb}$.

The total cross section of p-p interaction at our energy is $\sigma_{tot} = 37.5\,\mathrm{mb}$. The difference from the trigger one is caused by rejecting about 75 % of the elastic cross section and 30 % of the low-mass diffraction cross section by the trigger. [22]

3.2.2 Inclusive cross section σ_{inc}

The trigger cross section can be used as a normalization factor for evaluating inclusive cross sections. If one assume that the number of triggers is equal to N_{events}, the number of events recorded in μDST:

$$E\frac{d\sigma_{inc}}{d^3p} = \sigma_{tr}\ \frac{E}{\Delta p^3_{bin}}\frac{N^{bin}_{particle}}{N_{events}} \tag{3.3}$$

where $N^{bin}_{particle}$ is the number of particles within a kinematic region Δp^3_{bin}.

More details about the derivation of this formula can be found in [21] and [22].

3.3 Gas Ionization by Charged Particles

Whereas our method of identifying particles is based on specific energy losses of particles traversing TPCs, in this section, I will explain some basics about ionization losses and how we measure this quantity. The description of how to extract these numbers will follow in section 3.6 on page 19.

When a charged particle flies through the gas, it looses its energy because of random collisions with the gas atoms. We call the electrons knocked-out of the atoms due to these collisions the primary ionization.

However, most of the ionization produced along the particle track is caused by the secondary ionization, where the electrons are ejected from atoms not encountered by the primary particle. There are several processes contributing to the secondary ionization, such as collisions of ionization electrons with surrounding atoms or reactions involving intermediate excited states of the gas atoms (*Jesse effect*). For more details see [16].

3.3.1 Energy loss dE/dx

The average energy loss dE/dx of charged particles is described by the *Bethe-Bloch equation*. There are several representations of this equation, but they depend on many factors, which are extremely difficult to determine. We

use a parametrisation produced by *Gabor Veres* together with μDST, see Appendix C.

The Bethe-Bloch equation (BB) is a function of many factors and parameters, most of them are constants for a TPC. So our parameterized BB is a function of the particle's $\beta\gamma$. As different mass particles with the same momentum have different $\beta\gamma$, we can distinguish among them by means of dE/dx information. Figure 3.1 shows the momentum dependence of the dE/dx.

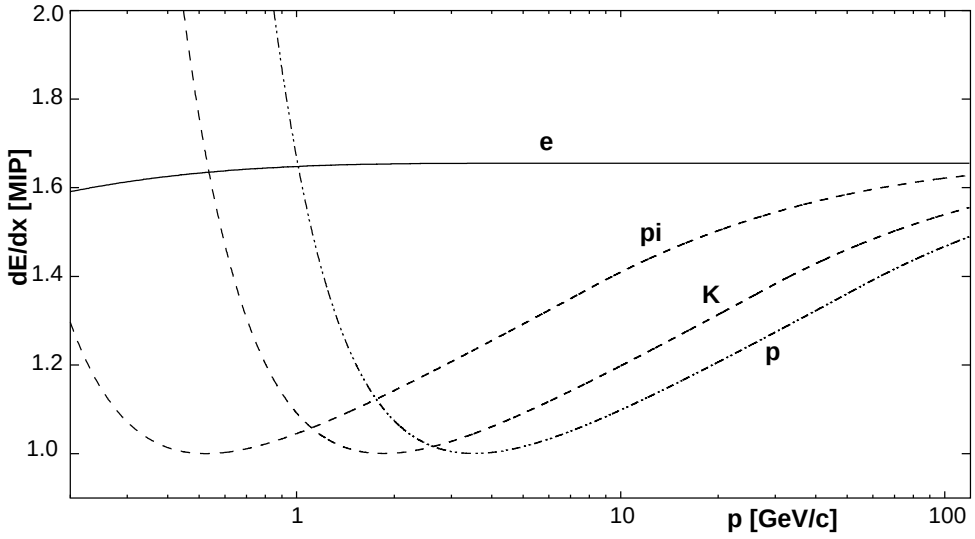

Figure 3.1: Bethe-Bloch curve for e, pi, K, p as a function of momentum. Vertical axis is normalized to minimum ionization (MIP).

The fluctuations of the dE/dx are described by the *Landau distribution*. This distribution differs from the Gaussian one by the long tail up towards the higher values due to the secondary ionization.

For more details about ionization losses see [16] or [17].

3.3.2 Truncated mean

The Landau distribution is complicated to parametrise. Therefore, the method of *truncated mean* is used for obtaining the mean value of a particle's ionization from its track samples. Calculation of the truncated mean in general means the following: order the samples by measured quantity, take some subset of these samples and average them, see [16], page 247.

As we measure dE/dx via the charges of the track's clusters, it means that the mean value of dE/dx is calculated as an average of some part of the ordered measured values of the track's cluster charges.

A MC simulation proved that the optimal choice is to average the first half of the ordered samples, which increases dE/dx resolution by typically

20 %. If the particle left enough track points in the detector, truncated mean values of particle ionization obeys a Gaussian distribution. [1]

3.4 Data binning

As our goal is to extract the cross sections, we are interested in particle flows into different phase space regions. For this purpose we must cut the phase-space into well defined pieces – *bins*. I have chosen the bins to be rectangular in the plane of transversal and longitudinal momentum in the laboratory frame: $< p_T; p_L^{lab} >$.

Proper binning is very important for the performance of the method for a couple of reasons. We need enough number of tracks in each bin. Otherwise, further described dE/dx fit does not work, and similar statistics in each of the bin helps to obtain comparable results in the bins. In the regions where the Bethe-Bloch functions for different particle species are overlapping, smaller bins produce better results, because, while averaging over the overlapping regions, discriminatory dE/dx information is lost.

The bins can be defined either manually or by some algorithm.

3.4.1 Manual binning

Manual binning have been used to define a well-tried set of 13 bins in $p_L^{lab} \in < 2; 50 >$ GeV, which are useful for comparing with results of other methods, models or other data. These bins lie in a region of high statistics – mean $\overline{p_T} =$ 400 MeV in these bins, as most of the pions are produced with transversal momentum around 400 MeV. Also, the old reconstruction chain produces minimum of split tracks and other biases in this region.

This binning is used for comparison with models in section 5.3 on page 45 and also for checking of the "development versions consistency".

The part of the phase space that is covered by it is shown on figure 3.2.

3.4.2 Binning algorithms

When all the phase space we analyze is to be binned, it is important to have similar statistics in each bin. To meet this requirement, hand-made binning is very painful and ineffective – the whole data has to be processed in order to calculate the number of tracks in each the bin ... So, I designed two algorithms for automatic binning, described in the appropriate section 4.2.1 on page 27.

3.5 Data cuts

We are not interested in all the tracks in the $<p_T, p_L^{lab}>$ bin. Firstly, we have to check for proper *charge* of the detected particles.

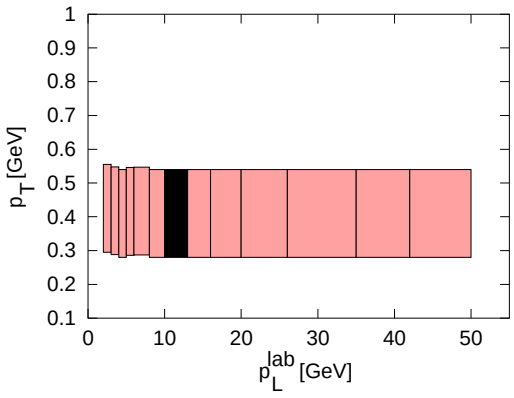

Figure 3.2: Manual binning – big bins of $\overline{p_T} = 400\,\mathrm{MeV}$ with many particles. For the dE/dx distibution of tracks in the black bin see figure 3.3.

Due to the acceptance reasons, we impose a φ *cut*[2] on the tracks, i.e. we take only the proper charge tracks within the $\pm\varphi$ sector, usually $\varphi = 50°$. Proper charge means that we take only those tracks which point in the direction their track is bent by the magnetic field. So if we analyze positive charged tracks, we take only tracks with $\varphi \in <310°, 50°>$, and for negative, $\varphi \in <130°, 230°>$.

Wrong charge tracks are detected by a much smaller area of the detector, because of the blind region in the middle of VTPCs and a gap between the MTPCs. Therefore, the uncertainty of their momentum and the possibility of being the decay tracks are much higher.

We also make a cut on the *number of points* used to reconstruct the track. Due to geometry considerations, all valid vertex tracks in analyzed phase-space must consist of more than 40 points. This will be discussed later in the section 5.4.2.. This cut rejects most of the split or trash tracks produced by the reconstruction chain.

Cutting on the number of track points also makes dE/dx information more reliable and the truncated mean distribution can be safely substituted by a Gaussian one.

Both these cuts are widely used by the members of NA49 collaboration who analyze μDST data, and their efficiency was tested and approved.

3.6 dE/dx fit method

The *dE/dx fit method* is based on fitting MC simulated dE/dx histograms (described later) to the experimental truncated mean distribution in some

[2] $\tan(\varphi) = p_y/p_x$; x is horizontal, y is vertical axis, z axis is a beam line

bin of the phase space.

$$\left(\frac{dE}{dx}\right)_{exp}^{hist}(i) \approx \sum_{j=1}^{4} a_j \cdot \left(\frac{dE}{dx}\right)_{MC_j}^{hist}(i), \quad j \in \{e, \pi, K, p\} \tag{3.4}$$

Figure 3.3 shows how the histogram of measured dE/dx can be fitted by simulated ones.

If the total number of the tracks in the bin is known, this number multiplied by the fit coefficients a_j gives the particle multiplicities $\overline{N_{particle}}$, from which one can calculate the inclusive cross sections.

This method is also described in [21].

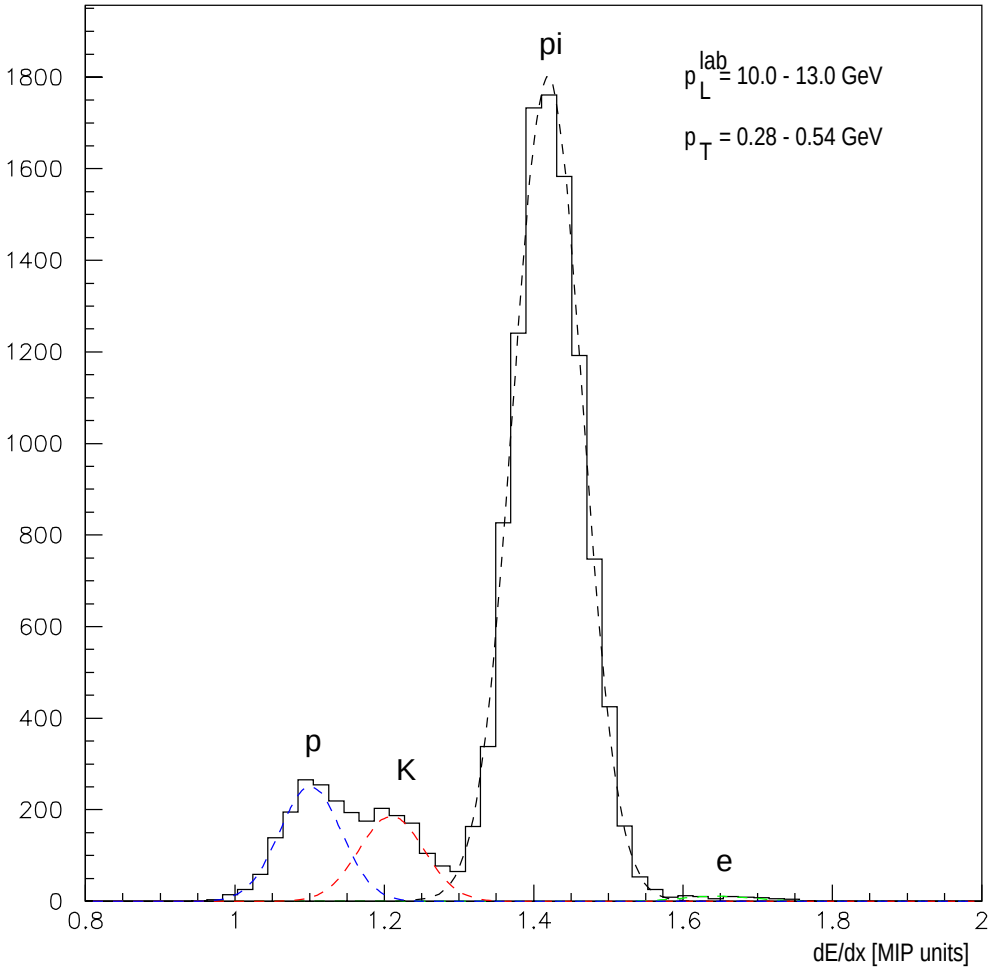

Figure 3.3: Histogram of measured dE/dx and fitted MC simulated dE/dx of positive charged particle tracks within laboratory momentum $p_L^{lab} \in < 10; 13 >$ GeV and transversal momentum $p_T \in < 0.28; 0.54 >$ GeV

3.6.1 Fit quality

Quality of the fit is appreciated by the variable χ^2, which is minimized by MINUIT [5] package:

$$\chi^2 = \frac{1}{N_{tracks}} \sum_{i=1}^{I_{lim}} \left[\left(\frac{dE}{dx} \right)_{exp}^{hist}(i) \; - \; \sum_{j=1}^{4} a_j \cdot \left(\frac{dE}{dx} \right)_{MC_j}^{hist}(i) \right]^2 \tag{3.5}$$

where I_{lim} is the number of histogram bins, N_{tracks} is total number of tracks.

To avoid confusion, I would like to stress that the χ^2 does not have a statistical significance of a common χ^2 variable. Our χ^2 is rather the residual sum of quadrates normalized to the number of tracks.

I tried to use the standard χ^2[3] variable, but the result of the fit is that the histogram bins which contain a low number of tracks are fitted well in detriment to highly occupied ones, due to the σ_i-normalization of the residual square in a common χ^2 fit. We do not want this fit behavior, since we are interested in the overall number of particles of some species in a fitted phase-space bin.

3.6.2 MC simulation of dE/dx

The aim of the *MC simulation* is to generate realistic (in our experimental environment) dE/dx distribution shape of detected particles in some $<p_T, p_L^{lab}>$ bin.

Beforehand, let us concentrate on the dE/dx information contained in the μDST. The value of the track's $(dE/dx)_{exp}$ contained in the μDST is evaluated as a weighted mean of the $(dE/dx)_i$ measured in the TPCs that the track particle passed through. Each $(dE/dx)_i$ is calculated as a truncated mean of the appropriate cluster charges. As the Bethe-Bloch function is different in the VTPCs and the MTPCs, the (dE/dx) measured in the MTPC is accordingly transformed.

The corresponding measurement error $\sigma_{exp}^{dE/dx}$ is basically a combination of relative the σ_is from different TPCs where the particle left the track.

$$\sigma_i \propto \frac{1}{\sqrt{N_i^{tr}}} \left(\frac{dE}{dx} \right)_i^{\alpha_i} \tag{3.6}$$

where $(\frac{dE}{dx})_i$ is the energy loss, α_i is an exponent ($\alpha_1 = \alpha_2 = 0.5$, $\alpha_3 = 0.7$) and N_i^{tr} is the number of the track's points in the i-th TPC.

According to the μDST author, accuracy of the α coefficients is very bad. Thus, we can *rescale* $\sigma_{exp}^{dE/dx}$ to $\sigma_{MC}^{dE/dx}$ using the square root (taking $\alpha = 0.5$) in formula 3.7 without making a big error.

[3] with σ_i^2 = content of the i-th bin of the dE/dx histogram

The Bethe-Bloch function appropriate for the global dE/dx in μDST is a result of a several-pass fit and calibration procedure. The final shape of the function is in Appendix C.2.

A detailed description of the method invented for evaluating global track's $(dE/dx)_{exp}$, its $\sigma_{exp}^{dE/dx}$, and the Bethe-Bloch function shape is explained in [18].

Suppose we measure some $(dE/dx)_{exp}$ of a track somewhere between a pion's and a kaon's line. Appropriate $\sigma_{exp}^{dE/dx}$ corresponds to the $(dE/dx)_{exp}$ ionization distribution with the maximum at this measured value.

We don't know which particle left the track in the detector, but we are sure that it was *either* a pion *or* a kaon *or* a proton *or* an electron, so the most probable dE/dx (maximum of the truncated mean distribution) is not a continuous variable, but for a given total momentum, it can have only four values for the mentioned particle species, given by the Bethe-Bloch equation: $(dE/dx)_{MC} = BB(p/m)$.

Since the value of the most probable ionization is not the measured one, and since the track's $\sigma_{exp}^{dE/dx}$ correspondents to the measured ionization, we also have to *rescale* the estimated distribution width:

$$\sigma_{MC}^{dE/dx} = \sigma_{exp}^{dE/dx} \cdot \sqrt{\frac{(dE/dx)_{exp}}{BB(p/m)}} \tag{3.7}$$

Generating MC histograms consists of the calculation of some number of MC entries for all the tracks in a bin. For each of the particle species we suppose that the track was left by it and we create corresponding MC events with a Gaussian distribution of the particle's energy loss at a given momentum p centered at $(dE/dx)_{MC} = BB(p/m)$ with corresponding $\sigma_{MC}^{dE/dx}$.

This way we get four MC histograms, $(dE/dx)_{MC_j}^{hist}$, $j \in \{e, \pi, K, p\}$, considering the track was made by an electron, a pion, a kaon and a proton.

3.7 Corrections

3.7.1 Bethe-Bloch shifts and σ_{rel}

The Bethe-Bloch function is only an approximation of a charged particle's energy loss, as the exact formula is unknown. For this reason, we introduce a new parameter(s), *Bethe-Bloch shift(s)*, which shifts the MC histograms.

Also the Gaussian shape is not the exact parameterization, even in the case of truncated mean, so we introduce next parameter(s), relative σ_{rel}(s), for fine-tuning of the width of MC distributions. For details see the programme code in Appendix D.

These shifts and σ_{rel}s are functions of the particle's momentum[4] and they are not independent. So, if one sets all of them as free parameters, the minimizing routine often blows up.

3.7.2 Weight factors and σ_{vertex}

When the reconstruction chain fits the *interaction vertex* of some event, the number of tracks in that event is very important for the success and accuracy of the fit – the less the number of tracks in the event, the broader the σ_{vertex}, the deviation of the vertex position definition, see [20].

The liquid hydrogen target is a cigar-shaped vessel with mylar windows on both the sides. Sometimes the incoming proton interacts with some nucleus of this mylar, mostly carbon. These trash events are thrown away by reconstruction chain by means of the vertex cuts[5], but the broader the σ_{vertex} is, the more events are dropped.

Sometimes for the low multiplicity events *the vertex can not be reconstructed at all* and these events are also dropped.

There are also so bad events, for which the reconstruction chain does not reconstruct any track. These are called *zero prongs*.

In all the cases we have triggered on that events, so we must correct for it. H. G. Fischer and Tanja Tsusa have studied these effects in the detail, the result of their effort are weight factors as a function of event's multiplicity.

3.7.3 Acceptance

Due to our cuts, in the most of analyzed region we have 100 % acceptance. However, some tracks with low longitudinal and high transversal momentum at the edge of the φ cut are not detected, because of the detectors geometry – tracks are too short and they are refused by cuts, or due to bugs in the reconstruction chain.

This can be cured by looking at the φ distribution of the tracks in given bin, which should be rectangular within the φ cut. If there is a statistically significant decrease of entries in the edge histogram bins, we can correct for it by multiplying the number of tracks in a bin with a ratio of the area of the should-be rectangle over the histogram area.

3.7.4 Feed over

We are interested in particles produced by the strong interaction, not in decay products of strange particles. Enhancement of particle yields due to this effect is called *feed over*.

[4] The reason is that particles with different momentum pass through different parts of the TPCs.

[5] Vertex cut for p-p events means, that the event is dropped if the vertex is not in inside the 11 cm middle part of the target, of which the full length is 14 cm.

Unfortunately, there is no way to account for feed over particles, because we have no reliable model predicting the production of these particles in our collisions. This contamination decreases with laboratory momentum, as the secondary vertices are further down the primary target. In the backward hemisphere, this effect competes with the feed down caused by acceptance losses, which makes this problem even more troublesome.

The solution for this problem is restricting ourselves to the projectile hemisphere, which is convenient in p-p interactions considering the collision symmetry.

Chapter 4

Description of Algorithms

In this chapter I would like to describe more deeply my approach to the algorithms used. The list of these programmes are enclosed in Appendix D.

4.1 Development remarks

After acquainting myself with the NA49 experiment, its methods and ways of research, my first analysis of invariant inclusive cross section (IIC) has started with FORTRAN code written by my supervisor, H. G. Fischer. This programme calculates IIC in one pre-defined bin with pre-defined values of Bethe-Bloch shifts and σ_{rel}s, processing the whole data set. For each experimental track it generates 10 MC tracks.

My task was to improve this method to be able to determine the shifts and σ_{rel} automatically, what was implemented in FORTRAN program `incl-pp.f`.

This program calculates IIC in 9×9 matrix of χ^2 according to equation 3.5 for 9 steps in common shift and common σ_{rel} and finds a minima of χ^2. Fitting of the histograms performs a hand-written minimization routine `FOURFIT` taken from the given code. Then it reduces the step of the shift and the σ_{rel} values and runs the next iteration. For each iteration, it scans the whole data set, and for each χ^2 matrix element, it calculates the MC tracks and fits them to the experimental distribution in a given bin.

In hindsight, the main benefit of this code was learning the FORTRAN language, understanding the dE/dx method, how it works in different phase space regions, the cuts used, and weight factors due to vertex resolution dependence on the events track multiplicity.

Consulting my effort with my consultant J. Dolejší, I was told about the MINUIT package[5]. After rewriting the code to use MINUIT, I have realized that the randomness of MC simulation brings along the dependence of χ^2 on the seed of random number generator[1], which was not observed in

[1] MINUIT calls this effect *time dependence*, i.e. the function is called with the same parameters, but the result is not the same.

previous algorithms used, as the seed was always the same.

To get rid of this dependence, I calculate once per bin, 10000 MC tracks per one measured and save them to larger histograms with $10\times$ smaller steps than the experimental one, assuming that shifts equal 0 and σ_{rel} equal 1. In each call, these histograms are properly transformed – shifted and rescaled, keeping the overall integral the same – to obtain MC histograms for fitting.

Results of this revision are the same due to small values of the shifts and σ_{rel} close to 1, but it is far much faster and versatile.

Data relevant for each bin are stored as ASCII files in a directory named by a bin definition[2]. This is inefficient and bulky, but as PAW NTUPLEs did not seem usable at the time, it was the only solution concerning the FORTRAN.[3]

Advancement of this treatment is a possibility of direct check of the results on the lowest level.

Together with developing the fitting routine, I have written programs which extract IIC values from the bin-directory structure and store them to a separate file for later analysis.

[2]For example, the directory containing information about bin at figure 3.3 in $p_L^{lab} \in <10;13>$GeV, $p_T \in <0.28;0.50>$GeV of positive tracks is named: `./pL:10.00,13.00_pT:0.280,0.540_Q:+1/`

[3]In my point of view, usage of the FORTRAN and the PAW is rather out-dated way of doing the job, more convenient tools appears to be c++ and the ROOT. Object oriented approach brings along many benefits and new possibilities, which will be discussed later. At this place I would like to note, that development of both the PAW and the ROOT is tightly linked to the NA49 experiment (or better, to Rene Brun).

4.2 Technique Used

The developed technique consist of several steps, which are displayed in figure 4.1. Algorithms corresponding to the diagrams in this figure are explained in the following sections.

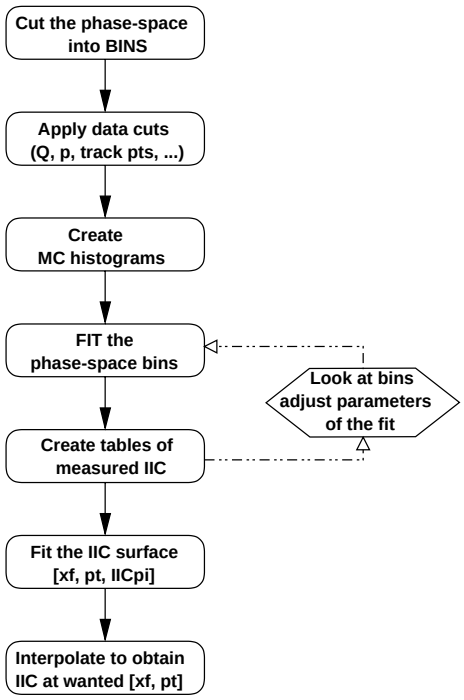

Figure 4.1: "Work flow" for extraction of the invariant inclusive cross sections.

4.2.1 Binning

Manual binning of some larger area of the phase-space is very tedious, so I have written two programmes, which automate this. The result of these programmes is the boundaries of the bins.

The first one – `phase_fit.f` and external function `ph_fcn.f` – was written in FORTRAN, and was inspired by the virtue of the MINUIT package.

Phase_fit is able to improve the $n \times n$ pre-defined hand-made binning via moving the bins boundary in order to minimize

$$\sum_{i=1}^{n \times n} (B_i - \overline{B})^2 \tag{4.1}$$

where B_i is the number of tracks in a bin i and $\overline{B}$ is the average of B_is. Pre-defined binning was manually adjusted[4] in p_T and logarithmic in p_L^{lab}, reflecting a nearly exponential decrease of pion yield in longitudinal momentum.

Minimization is performed by the MINUIT. $(n-1)\times(n-1)$ parameters, "cutting lines", are used. The problem of this algorithm is the substantial irregularity of particle distribution in phase-space, see picture 4.2.

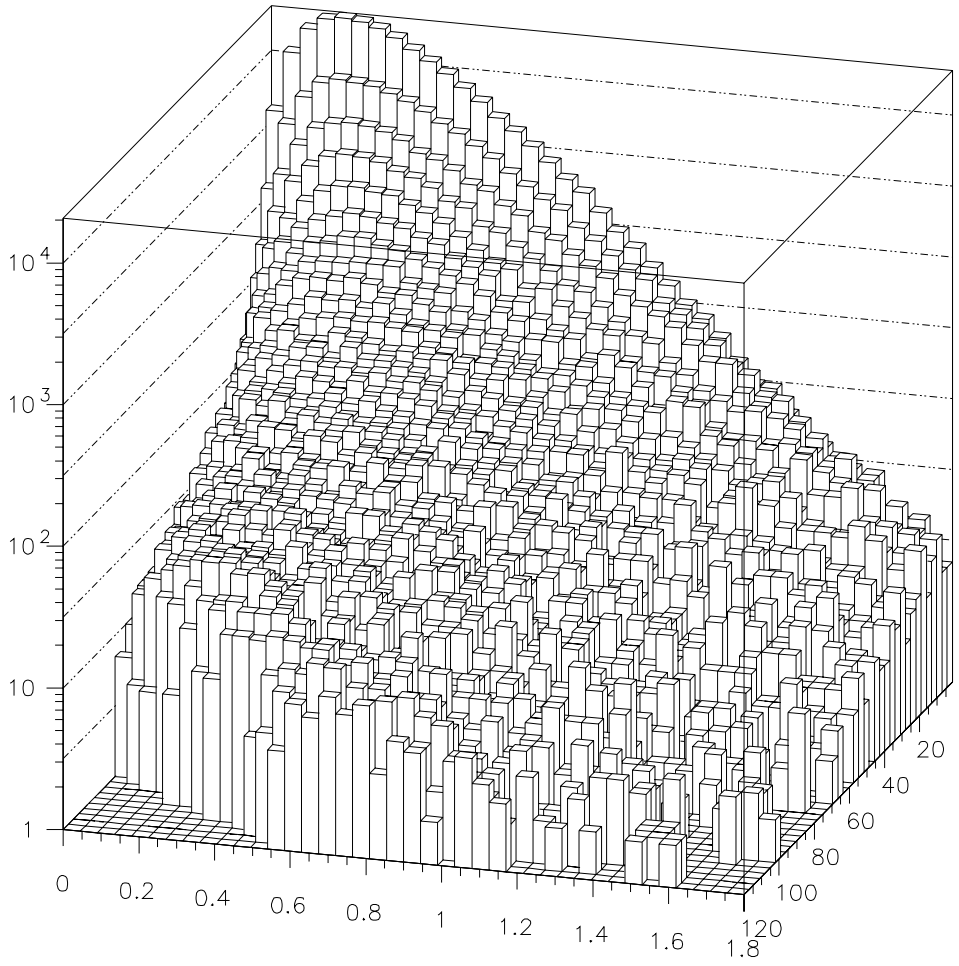

Figure 4.2: Histogram of all the tracks in the μDST that satisfy the data cuts. $p_L^{lab} \in < 1.5; 100 >$ GeV, $p_T \in < 0; 1.8 >$ GeV

In my opinion, any attempt at $n \times n$ binning produces many bins with several thousands of tracks and even more bins on the edges of the phase-space with less than one hundred of entries. This could be cured by manual

[4] p_T distributions obey the rule of $p_T \times exp^{-p_T^2}$ (with appropriate constants) in the first approximation. However, there is no inverse function to this formula.

joining of under-populated bins to the larger ones.

The second automated binning method – `bin_me.C` – was written in c++[5], because of the convenience of object-oriented programming. `Bin_me` is a recursive sorting code, that creates rectangular bins with equal statistics of tracks, and was inspired by the JPEG compression of images.

The core of the `bin_me` code is a self-calling procedure, `sortall`. `Sortall` decides if the array of tracks it operates on contains more than some minimum of entries. If it does the procedure sorts them by p_T or p_L^{lab}, depending on which side of the bin is "wider", cuts them into two halves and passes them to itself. If the array of tracks it is called with contains less tracks than some constant, the corresponding bin is written out, and the procedure exits to the lower level of recursion, and so on until all the phase-space has been binned.

Due to the different amount of positively and negatively charged tracks, we cannot obtain the same number of tracks in a bin for these two cases, see examples of the binning in figure 4.3. However, the bins of the same charge differ only by one track.

4.2.2 Data cuts

The second stage consist of preparing proper data in each of the bins – selecting the tracks that fall into bins and matching the cuts explained in section 3.5, page 18.

There is a code named `read_and_cut.f` for this purpose. It reads file `cuts.cfg` for the bin definition, and in then scans the μDST for the corresponding tracks, pre-calculates track values needed for later analysis and mean values of p_T, p_L^{lab}, x_F, y, ... in the bin, and saves it to the bin directory.

Human readable information about the bin contents is stored in file `cuts.out`, and information about the tracks and the bin for later computer analysis is contained in the file `cuts.dat`.

4.2.3 MC simulation and fitting

The core of the used method, MC simulation of dE/dx and fitting of the histograms, is contained in programme `minfit.f` and external function `fcn.f`. `Minfit` is a MINUIT calling code, and all the functionality is contained in the external function.

MINUIT calls the function with the set of parameters and some flag, used to control the function operation. Varying the parameters, it obtains some values of χ^2. Based on this knowledge, it tries to find the best fit values of the parameters.

[5] I would like to thank my friend *Martin Jelínek* who helped me write the code because of my inexperience with c++

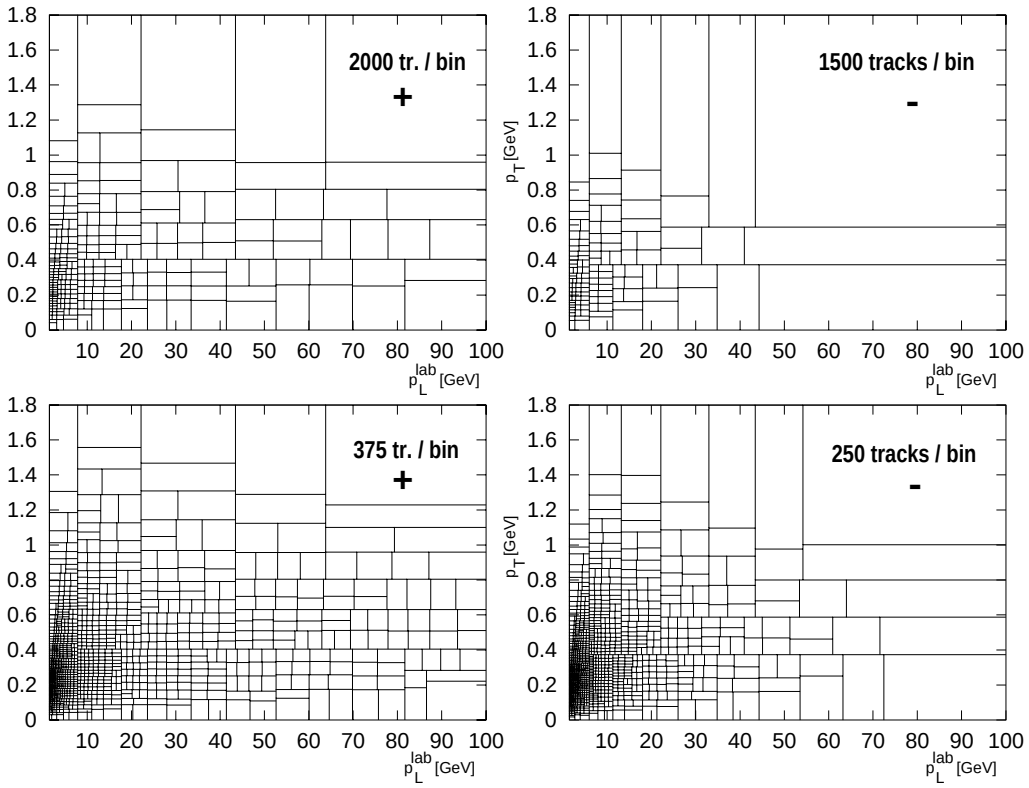

Figure 4.3: Binning produced by `binme.C` demanding at least 2100/400 tracks for halving the bin are on the upper/lower picture; these binnings are named E/C in the table 5.1 page 36. The left/right graphs corresponds to positively/negatively charged tracks.

Standard flag values are 1 for initializing, 2 for normal operation and 3 for the last call.

While initializing, the function reads the bin definition from file `fit.cfg` and the bin data from file `cuts.dat` located in the bin directory. It checks for the file `hist.dat`, which contains MC simulated histograms for the bin. It then either reads it or performs MC simulation based on the read experimental tracks and saves the simulated data.

In every call the function transforms generated MC distributions to the ones with the same binning as the experimental one has according to the fit parameters. Then it calculates the χ^2.

If the function is called with flag 3, in writes out the best-fit results to files `fit.out` and `fit.dat`, and dE/dx histograms to file `hist.hbk` in the bin directory.

The file `fit.out` contains human readable information about the bin content: mean values of kinematic variables, calculated values of IIC, fit parameters, value of $\chi^2 \times 100$ and fitted dE/dx histograms in ASCII format.

This file is accessible from the web script further described in section 4.2.6 on page 34.

There are twelve parameters to be fitted – four for particle fractions (amplitude of the distributions), four for the shifts, and four for σ_{rel}s. As they are correlated[6], it is impossible to fit them all together from the beginning.

For controlling the number of fit parameters, there are two flags – 10 and 11 – working as switches. The first one fixes the shifts, so there is only one "global" shift for all the MC histograms. The next call releases the shifts. Calling the function with flag 11 does the same for σ_{rel}.

According to my experience, the best results are obtained if both the shifts and σ_{rel}s are fixed for several minimization trials, then either the shifts or σ_{rel}s are released for several next trials.

During the minimization, it is very useful to see the fit results. For this purpose there are two flags – 20 and 21. Calling with 21 writes information about the fit to the screen. Calling with 20 writes relevant histograms, executes PAW to create a picture like 3.3, and displays it. There are different particle distributions distinguished by color in the picture, so one can clearly see the fit.

For processing more bins, `minfit` (and also `read_and_cut`) can be run in a batch, processing all the bins in some common way of the minimization calling proceeding, and problematic bins can then be processed by hand.

4.2.4 Extracting the results from bin directories

When all the bins are fitted, the information about the fit results is interspersed among the bin directories. To collect relevant results, programme `cross.f` is used.

This code scans all the directory bins, reads files `fit.dat` and writes out needed values of IIC to the files. It produces some files for later analysis and also a table that simplifies finding of the bins where the fit did not work. These tables are usable only in the case of $n \times n$ binning produced by `phase_fit` code, otherwise we use the technique described in the following section.

4.2.5 Fitting IIC surface

If we are interested in some value of IIC out of the measured points, it is necessary to *interpolate measured values*. This could be done either locally (in proper sense of interpolation) or globally; I will focus the global fit first. The value of the difference between the fit function and the measured points can also be significant for such bins, where the dE/dx fit failed.

[6]This problem is clearly seen on figure 3.3 considering the proton and kaon peaks, as they are about the same size in most of the phase space.

In my opinion, the best solution is a standard χ^2 fit of a function $f^\pi = f(x_F, p_T; c_j)$ to measured values of cross section $\rho_i^\pi \equiv E\, d^3\sigma_{inc}^\pi/dp^3$ at points $[x_F, p_T]_i$ via adjusting the parameters c_j.

We have to choose some fit function shape for this purpose. According to the literature [6], [11], [7], [12], [13], ..., at a fixed interaction energy the invariant cross section can be factorized – approximated as a product of two terms, each one depending on one of the independent variables:

$$f^\pi(x_F, p_T) = F(x_F) \cdot G(p_T) \tag{4.2}$$

These functions are commonly parameterized by the following formulae:

$$\begin{aligned} F &= c_1 \cdot (1- \mid x_F \mid)^{c_2} \\ F &= c_1 \cdot exp(c_2 x_F^2) \\ G &= c_1 \cdot exp(c_2 p_T) \\ G &= c_1 \cdot exp(c_2 p_T^2) \\ G &= c_1 \cdot exp(c_2 \sqrt{m_\pi^2 + p_T^2}\,) \end{aligned}$$

More parametric fits are usually combinations of the above functions and their variations.

After some experimentation with different shapes of the fit function f^π, including even non-factorizable terms, I have realized that the value the function 4.4 is very similar for most of the fit formula shapes, so the actual selection is to a large extent a matter of choice.

I have chosen the simplest form, which still reproduced the data values quite correctly in my point of view:

$$f^\pi(x_F, p_T) = c_1 \cdot exp(c_2 p_T + c_3 p_T^2 + c_4 p_T^4) \cdot (1- \mid x_F \mid)^{c_5} \tag{4.3}$$

Having no reliable information about the measured points error, one can fit 4.3 without any errors, just summing the deviations squared. This solution is not good enough because the range of measured values is about five orders.

For this purpose, we can include some kind of "statistical" error:

$$(\sigma_i^{stat})^2 = (\rho_i^\pi)^2/N_i^\pi$$

where N_i^π is the number of pions in the bin i.

The fit's χ^2 is then calculated by the following standard formula[7]:

$$\chi^2 = \frac{1}{N_i - N_j} \sum_{i=1}^{N_i} \Big(\frac{f^\pi(x_F, p_T; c_j)_i - \rho_i^\pi(x_f, p_T)_i}{(\rho_i^\pi)^2/N_i^\pi} \Big)^2 \tag{4.4}$$

[7] As the sum of normalized deviations squared is divided by the number of degrees of freedom, this variable is commonly marked χ^2/NDF.

where N_j is the number of the fit parameters and N_i is the number of measurements (bins).

The χ^2 obtained by formula 4.4 is not satisfactory. Even after rejecting some badly fitted bins, the value of χ^2 is from 10 to 60, depending on the binning. The reason is that we do not figure in systematic errors, and also the fit function does not describe measured dependence perfectly.

If we believe in the fit function, there is a possibility to estimate the systematic error: if our errors would be correctly established, the mean value of χ^2 is expected to be equal one. Assuming that relative systematic error is the same for all the measurements, we can introduce a new parameter, *average relative systematic error*, σ_{ASE}:

$$\chi^2 = \frac{1}{N_i - N_j} \sum_{i=1}^{N_i} \Big(\frac{f^\pi(x_F, p_T; c_j)_i - \rho^\pi(x_f, p_T)_i}{(\rho^\pi)^2 \cdot (1/N_i^\pi + \sigma_{ASE}^2)} \Big)^2 \tag{4.5}$$

The value of σ_{ASE} can be obtained iteratively:[8] first we fit the function to measurements figuring in only statistical errors, then we fix these parameters and fit the σ_{ASE} to make χ^2 equal one, and again fit the parameters c_i, and so on. It takes about three iterations to obtain stable values.

The fit is performed by MINUIT called from the programme `intfit.f` and the corresponding function `int.f`. Measured points for the fit are read from a file created by code `cross.f`. Only the points with $x_F \in < -.015, 0.55 >$ are concerned due to the acceptance reasons.

This code also allows displaying the measurements, their variance and maximal deviation by flag 11, and rejection of certain measurements by some maximum allowed variance by flag 13. Flag 14 serves as a switch between fitting parameters c_i and σ_{ASE}. Flag 12 causes writing out of actual fit parameters to file `fitpar.pi` and not-rejected measurements to file `re-fit.pi`. This allows online fit checking by eye using some plotting software (e.g. *gnuplot*).

4.2.6 Interpolating IIC values

If we are interested in the value of IIC at some point $[x_F, p_T]_0$, using the value of the interpolating function at this point is not the best idea, because the function shape is just an approximation.

A better solution is using the weighted average of several N_{pts} measurements closest to $[x_F, p_T]_0$, continued to this point by means of the slope of the interpolation function, i.e. weighted average of values:

$$\rho_j^\pi = \rho^\pi(x_F, p_T)_i - f^\pi(x_F, p_T)_i + f^\pi(x_F, p_T)_0 \tag{4.6}$$

[8] If one tries to fit σ_{ASE} together with c_i, the fit blows up.

Weights for the average are distances of measurements from $[x_F, p_T]_0$. The error is calculated by the standard formula:

$$\frac{1}{\sigma_\rho^2} = \sum_{j=1}^{Npts} \frac{1}{\sigma_j^2} \tag{4.7}$$

where the measurement errors are estimated as a sum of the statistical error and the "average systematic error" determined by 4.5:

$$\sigma_j^2 = \frac{(\rho_j^\pi)^2}{N_j^\pi} + (\rho_j^\pi \cdot \sigma_{ASE})^2 \tag{4.8}$$

Programme `tellme_ic.f` is intended to find out IIC in any $[x_F, p_T]_0$ point within the analyzed phase-space based on the specified number of the closest measurements. It is used as a core of a Perl script[9], which presents the interpolated value of IIC and also the measured points used in a table and a graph.

Programme `table_ic.f` serves for evaluating IIC and specified points $p_T \in \{0.2, 0.4, \ldots, 1.2\}$ GeV and $x_F \in \{0.05, 0.1, \ldots, 0.4\}$ for comparison with the ISR data.

4.2.7 Binning comparison and Acceptance check

For the purpose of comparing the results of IIC obtained by different binnings and for checking tracks φ-distribution, there is a code `statbins.f`.

Original motivation for writing this programme was comparison of the results by looking at the differences between the averaged value of IIC in the "biggest" bin and measured values in corresponding bins of all the binnings (the bins of "smaller" bins are sub-bins of the "bigger" ones). Unfortunately, this comparison does not work because the dependence of IIC is very steep.

The useful part of this programme is a subroutine `phistat`, which checks whether the φ-distribution of the tracks is flat by means of χ^2_φ :[10]

$$\chi^2_\varphi = \frac{1}{N^{\varphi bins} - 1} \cdot \sum_{i=1}^{N^{\varphi bins}} \frac{\left(N_i^{tracks} - (N^{tot}/N^{\varphi bins})\right)^2}{N_i^{tracks}} \tag{4.9}$$

where $N^{\varphi bins}$ is the number of bins in φ, N_i^{tracks} is the number of tracks found in the i-th φ bin, and N^{tot} is the total number of tracks in an investigated phase-space bin.

[9] located at `http://www.amu.cz/cgi-bin/iic/iic.pl`

[10] As divided by the number of degrees of freedom, somebody may prefer to call it χ^2_φ/NDF

4.3 Comparison with models

Measured invariant inclusive cross sections of pions have been compared with two event generators – Fritiof 7 [28] and Nexus 2.00beta[11] [30].

The Fritiof data set has been created and provided to me by *Bozena Boimska*, a member of NA49 collaboration. The file contains 400 000 inelastic p-p events, generated under NA49 conditions – incoming proton energy is 158 GeV, events are recorded in the laboratory frame.

The Nexus events were generated by me, using the latest version available, 2.00beta[12]. This version had to be patched in order to display the parent particle IDs. The data set contains same number of events as the Fritiof one.

There is a FORTRAN programme, named `generators_ic.f`, that extracts the IIC values in defined bins from both the output types by simple counting of the particles. The program code is different only in the reading section, which makes the comparison easy.

Proper normalization of obtained values is very important. As there is only on inelastic reaction channel contained in both the Nexus and Fritiof models, the results are normalized assuming 31 mb as the total inelastic cross section at our energy[13].

[11] Nexus is the follower of Venus event generator created by K. Werner. [29]

[12] It takes about 0.45 s to generate one proton–proton event on an AMD K6/2 at 350 MHz by means of this generator.

[13] Total cross section is 37.5 mb. Elastic component is about 17.5 % of the total one, σ_{el} = 6.5 mb.

Chapter 5

Results

In this chapter the results are presented and discussed.

5.1 Extracted data

Due to sizable differences in the pion density over the whole accessible phase-space, see figure 4.2 on page 28, we have to resign any $n \times n$ binning, so only the binnings produced by `binme` algorithm are discussed in the following.

I have chosen six different binnings with different amounts of particle tracks, as shown in figure 5.1 in order to check stability of the method.

binning	pos. tracks	neg. tracks
A	94	63
B	188	125
C	376	250
D	751	500
E	1503	2000
F	3006	4000

Table 5.1: Average number of tracks per bin for different binnings used.

There are several effects concerning the number of particle tracks in the bin. It is clear that the less tracks we have, the bigger the statistical variance; we also need some minimal number of tracks in the bin to be able to fit them using the dE/dx method – lowering the bin size increases the error of determining the IIC value. On the other hand, the more tracks in the bin, the bigger the uncertainty of $\overline{x_F}$ and $\overline{p_T}$.

The important effect specific to our method is the following: if we increase the bin size, we decrease the dE/dx resolution, because particles with different momenta have different dE/dx according to the Bethe-Bloch function (figure 3.1 page 17).

The results of the fits 4.5 are presented on the following two pages for all the binnings. Values of IIC in these bins ware obtained by simultaneous dE/dx fit of only six parameters – four for the particle ratios, common (parallel) shift and common σ_{rel}. This produces only a little error, as the pions are the most populated particles.

5.1.1 Fit parameter tables - positive tracks

binning A		
parameter	value	error
c_1	47.67	68.8
c_2	-1.92	8.7
c_3	-3.19	11.3
c_4	0.57	2.8
c_5	4.99	2.4
N_{bins}^{all}	3611	
N_{bins}^{used}	3542	
accepted	98.1 %	
σ_{ASE}	32.9 %	

binning B		
parameter	value	error
c_1	56.83	54.1
c_2	-2.34	5.4
c_3	-2.93	7.1
c_4	0.56	1.9
c_5	4.95	1.8
N_{bins}^{all}	1804	
N_{bins}^{used}	1770	
accepted	98.1 %	
σ_{ASE}	25.7 %	

binning C		
parameter	value	error
c_1	59.45	49.8
c_2	-2.30	5.1
c_3	-3.19	7.0
c_4	0.71	2.0
c_5	4.73	1.6
N_{bins}^{all}	900	
N_{bins}^{used}	882	
accepted	98.0 %	
σ_{ASE}	21.2 %	

binning D		
parameter	value	error
c_1	59.03	46.9
c_2	-2.23	4.8
c_3	-3.36	6.8
c_4	0.79	2.2
c_5	4.45	1.4
N_{bins}^{all}	451	
N_{bins}^{used}	430	
accepted	95.3 %	
σ_{ASE}	19.1 %	

binning E		
parameter	value	error
c_1	57.71	45.5
c_2	-2.32	4.9
c_3	-3.07	6.8
c_4	0.61	2.0
c_5	4.43	1.3
N_{bins}^{all}	225	
N_{bins}^{used}	218	
accepted	96.9 %	
σ_{ASE}	19.5 %	

binning F		
parameter	value	error
c_1	63.55	48.3
c_2	-2.60	4.8
c_3	-2.85	7.0
c_4	0.55	2.4
c_5	4.43	1.3
N_{bins}^{all}	111	
N_{bins}^{used}	105	
accepted	94.6 %	
σ_{ASE}	17.8 %	

5.1.2 Fit parameter tables - negative tracks

binning A		
parameter	value	error
c_1	42.43	21.9
c_2	-1.70	3.0
c_3	-3.72	4.1
c_4	0.73	1.1
c_5	5.80	1.5
N_{bins}^{all}	3626	
N_{bins}^{used}	3561	
accepted	98.2 %	
σ_{ASE}	43.9 %	

binning B		
parameter	value	error
c_1	50.73	40.3
c_2	-2.04	4.8
c_3	-3.57	6.6
c_4	0.74	1.8
c_5	6.23	2.5
N_{bins}^{all}	1814	
N_{bins}^{used}	1738	
accepted	95.8 %	
σ_{ASE}	18.7 %	

binning C		
parameter	value	error
c_1	50.72	40.2
c_2	-2.11	4.9
c_3	-3.50	6.9
c_4	0.75	2.0
c_5	6.11	2.5
N_{bins}^{all}	907	
N_{bins}^{used}	879	
accepted	96.9 %	
σ_{ASE}	19.0 %	

binning D		
parameter	value	error
c_1	52.77	33.2
c_2	-1.76	4.2
c_3	-4.31	6.5
c_4	1.10	2.5
c_5	6.53	1.9
N_{bins}^{all}	228	
N_{bins}^{used}	218	
accepted	95.6 %	
σ_{ASE}	15.4 %	

binning E		
parameter	value	error
c_1	55.76	31.6
c_2	-1.83	4.1
c_3	-4.44	6.7
c_4	1.22	3.2
c_5	6.87	1.6
N_{bins}^{all}	113	
N_{bins}^{used}	109	
accepted	96.5 %	
σ_{ASE}	13.4 %	

binning F		
parameter	value	error
c_1	63.30	32.8
c_2	-2.34	3.9
c_3	-3.60	6.6
c_4	0.48	3.4
c_5	7.91	1.4
N_{bins}^{all}	56	
N_{bins}^{used}	54	
accepted	96.4 %	
σ_{ASE}	11.5 %	

5.1.3 Discussion

The fit parameters of different binnings embodies noticeable mutual agreement, though their absolute one-standard deviation errors for each fit are enormous.

This correspondence is shown on table 5.2 for the binnings B, C, D and E. The fit parameters of binnings A and F are much different, so we can assume them as a boundaries for the binning play-ground.

	positives		negatives	
parameter	average	error	average	error
c_1	58.43	1.3	52.50	2.1
c_2	-2.30	0.04	-1.94	0.14
c_3	-3.14	0.14	-3.71	0.77
c_4	0.67	0.08	0.96	0.21
c_5	6.64	0.2	6.44	0.3

Table 5.2: The average and standard error of parameters for binnings B, C, D, E.

5.1.4 Binning C

I have chosen binning C as the optimal choice. This binning is also used by the web script mentioned in 4.2.6 page 34 and for the comparison with literature data in 5.2.

Figures 5.1 and 5.2 show the measurement points, obtained IIC, and the fit function shape for π^+ and π^-.

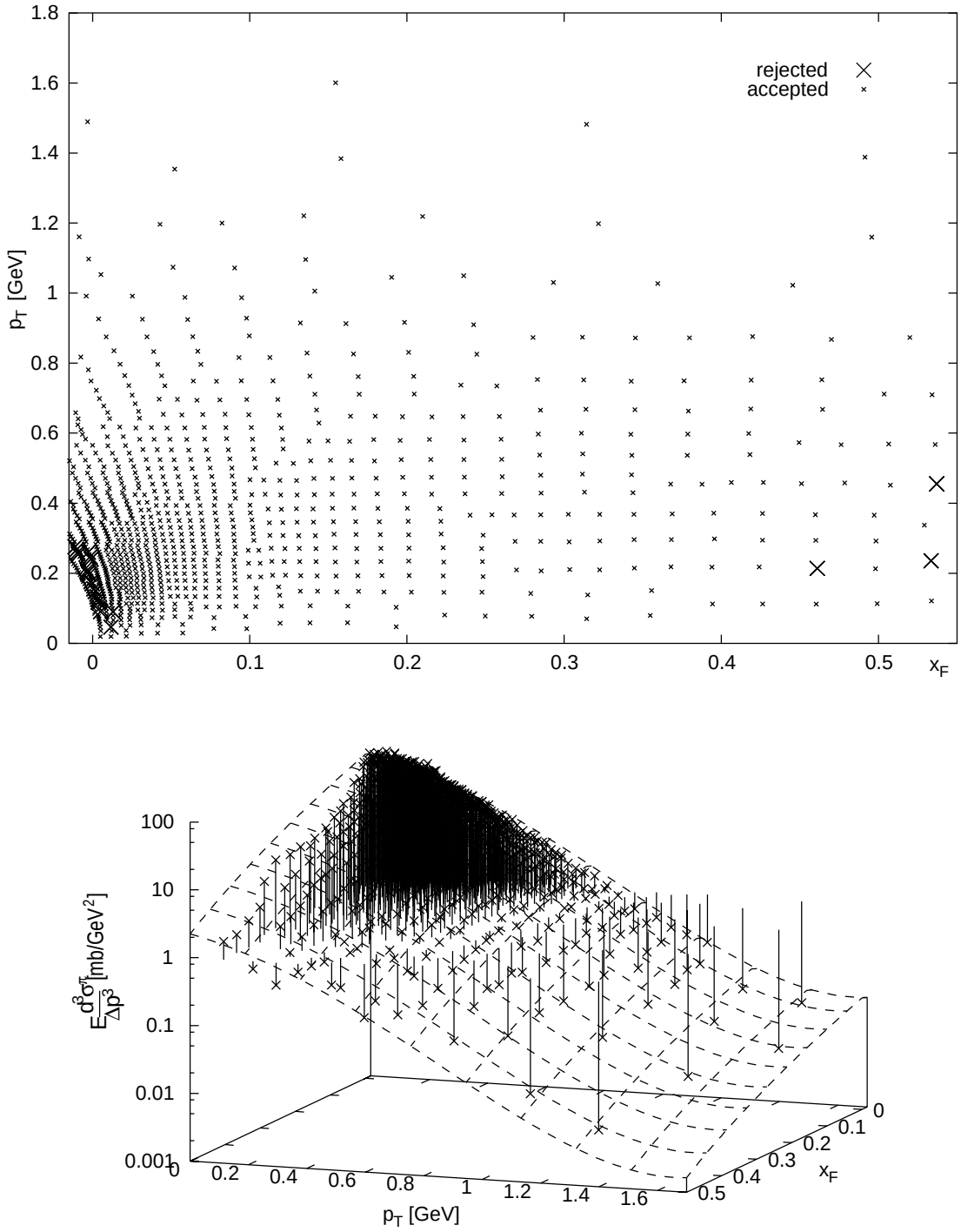

Figure 5.1: Top – centers of positive bins $[x_F, p_T]_i$ for binning C, rejected and accepted bins are shown. Bottom – measured values of invariant cross section of positive pions in the bins (lines from 1 to cross at the measured value) and the fit function (surface).

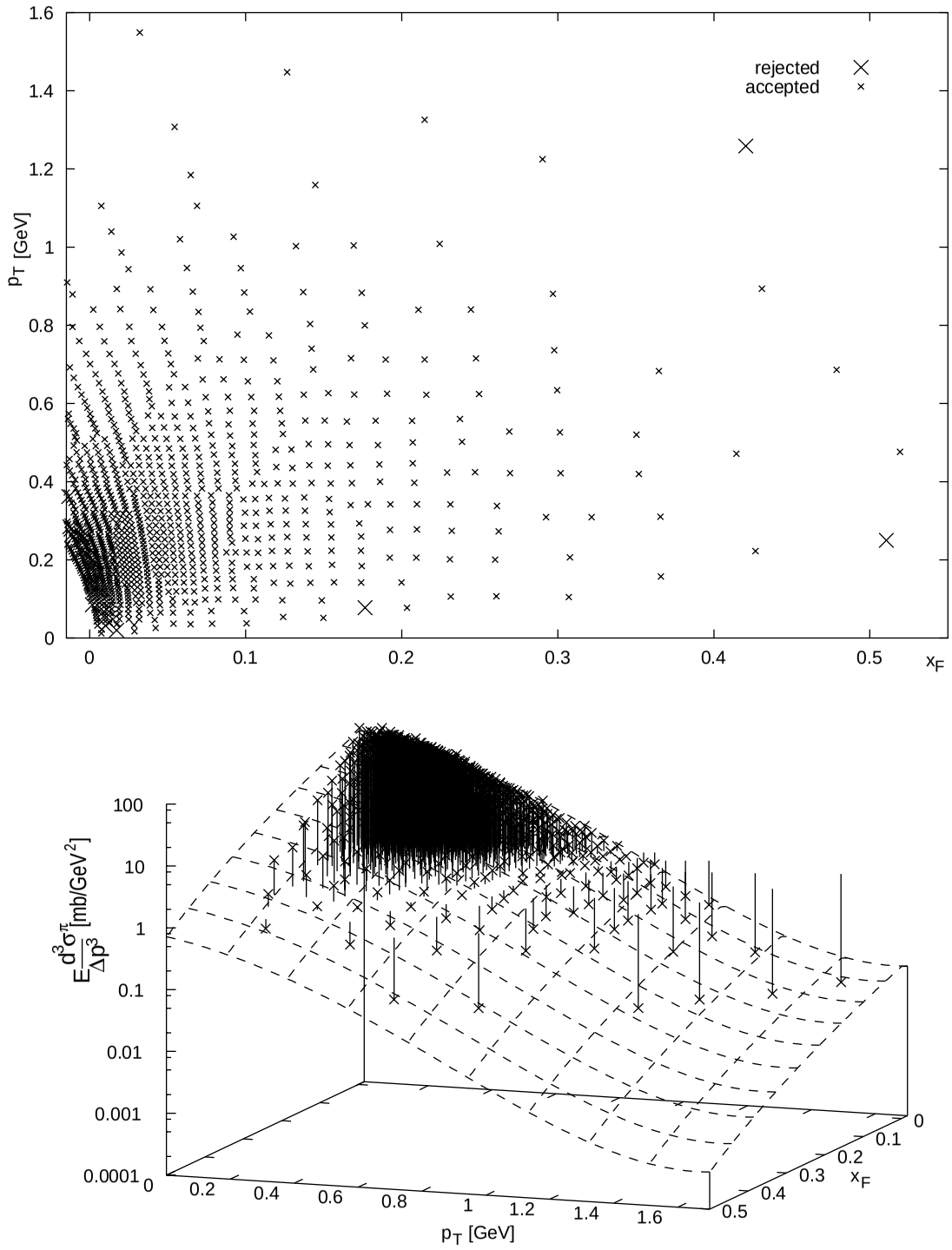

Figure 5.2: Top – Centers of negative bins $[x_F, p_T]_i$ for binning C, rejected and accepted bins are shown. Bottom – Measured values of invariant cross section of negative pions in the bins (lines from 1 to cross at the measured value) and the fit function (surface).

5.2 Comparison with the data in literature

For the purpose of comparison with the ISR data, the `table_ic` algorithm was used to produce interpolated values at suitable $[x_F, p_T]$ points: $p_T \in \{0.2, 0.4, \ldots, 1.2\}$ GeV and $x_F \in \{0.05, 0.1, \ldots, 0.4\}$.

The IIC values were obtained by use of the three closest measurements from the binning C.

The ISR data was given to me by H. G. Fischer as a result of his scan over existing data, and is based mainly on [14] and [15]. These data are, up to my knowledge, the most representative currently known values of IIC. Although they are displayed as straight lines without error bars, errors presented in these publications are about 5–30 %.

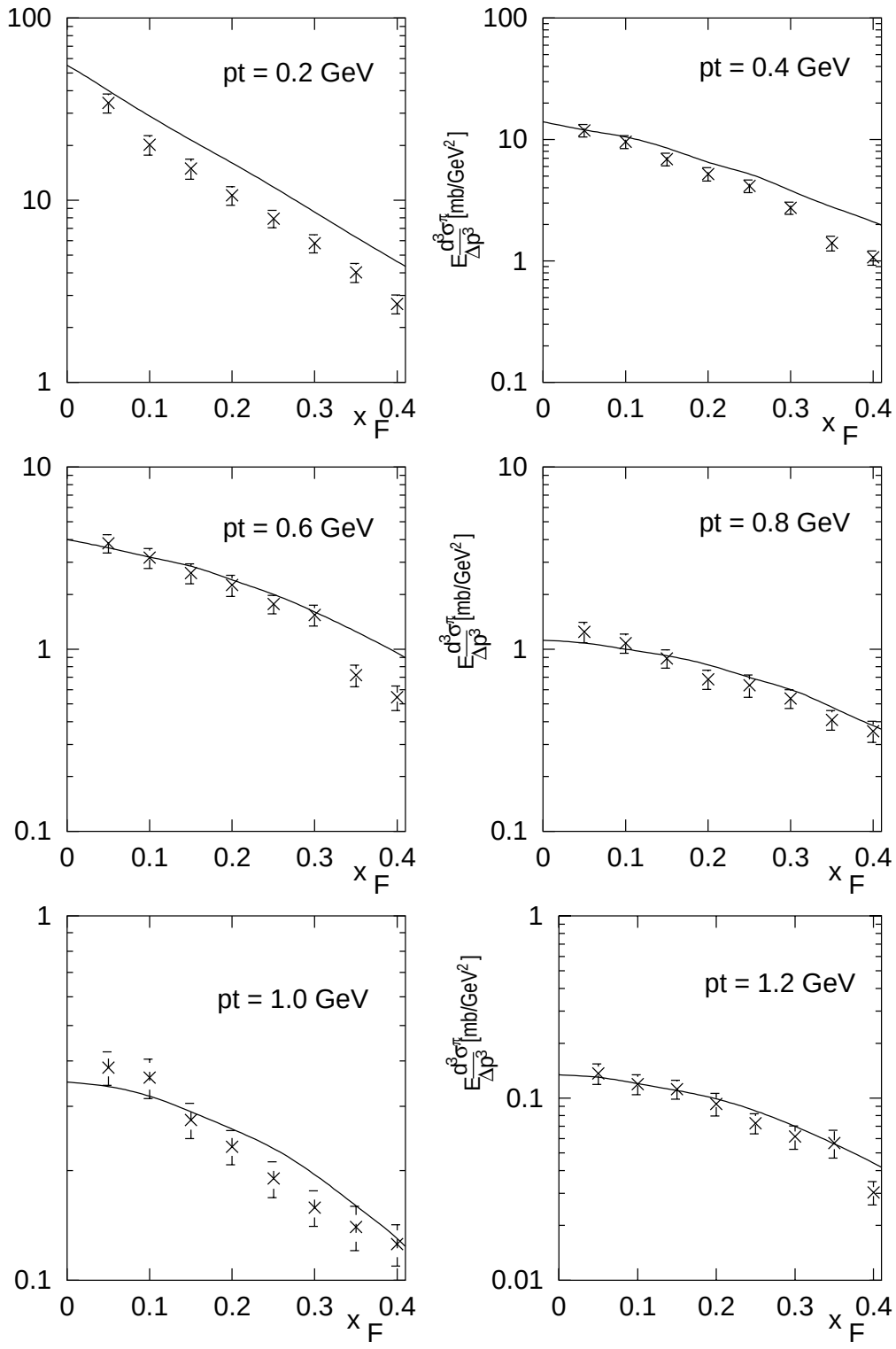

Figure 5.3: Comparison of evaluated invariant inclusive cross section of π^+ (points) with the ISR data (lines).

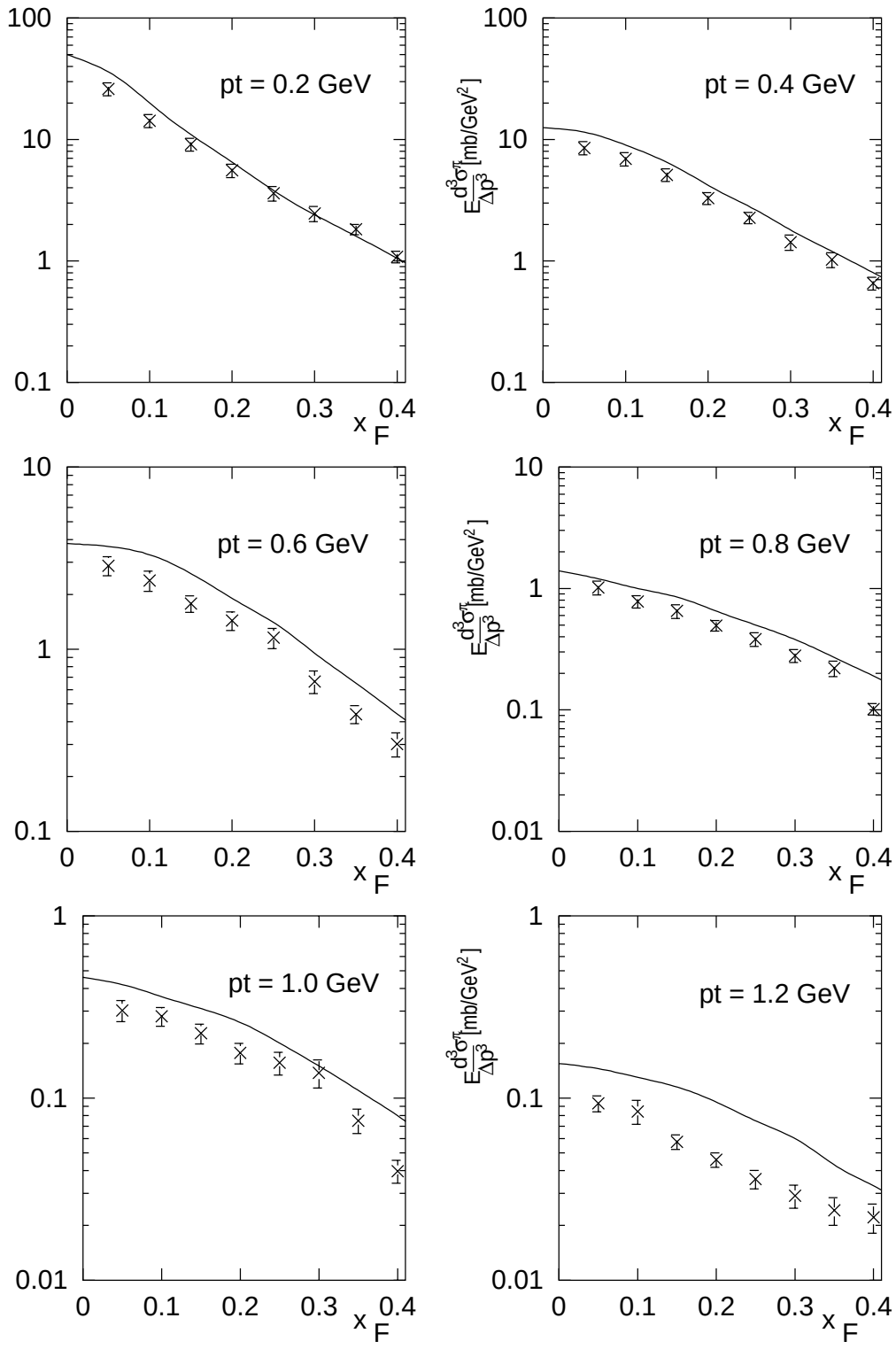

Figure 5.4: Comparison of evaluated invariant inclusive cross section of π^- (points) with the ISR data (lines).

5.3 Comparison with Event Generators

5.3.1 Manually defined bins

Figure 5.5 compares IIC obtained from the data file, events generated by Nexus 2 and Fritiof 7.

These values of invariant inclusive cross section were calculated by the adjustment of all the 12 parameters of the dE/dx fit. The influence of different number of the dE/dx fit parameters on the results is discussed in the section 5.4.1 on page 47.

It is clearly visible from figure 5.5 that Nexus 2 generated data are much closer to the observed dependency than the Fritiof 7 ones.

5.3.2 Automated binning

The IIC values obtained from both the Nexus 2 and Fritiof 7 generated events were interpolated and fitted using the same procedure as the experimental ones, as explained in 4.2.5, i.e. using formula 4.5, but without rejection of any bin. The binning C has been used.

The results of the interpolation function fit are displayed at the tables 5.3 and 5.4.

Nexus positives		
parameter	value	error
c_1	62.06	27.5
c_2	-2.11	2.7
c_3	-3.36	3.7
c_4	0.60	1.1
c_5	5.20	0.9
N_{bins}	902	
σ_{ASE}	11.8 %	

Nexus negatives		
parameter	value	error
c_1	46.72	19.3
c_2	-1.64	2.5
c_3	-3.77	3.6
c_4	0.68	1.1
c_5	6.16	1.4
N_{bins}	906	
σ_{ASE}	10.6 %	

Table 5.3: Fit 4.5 parameters of Nexus 2 generated data, binning C

Comparing the tables 5.3 and 5.4 with the corresponding tables of data fit parameters shows that the parameters of the Nexus 2 data fits are closer to the data ones than the Fritiof 7 ones, but this difference is not as significant as in the case of the comparison presented in figure 5.5.

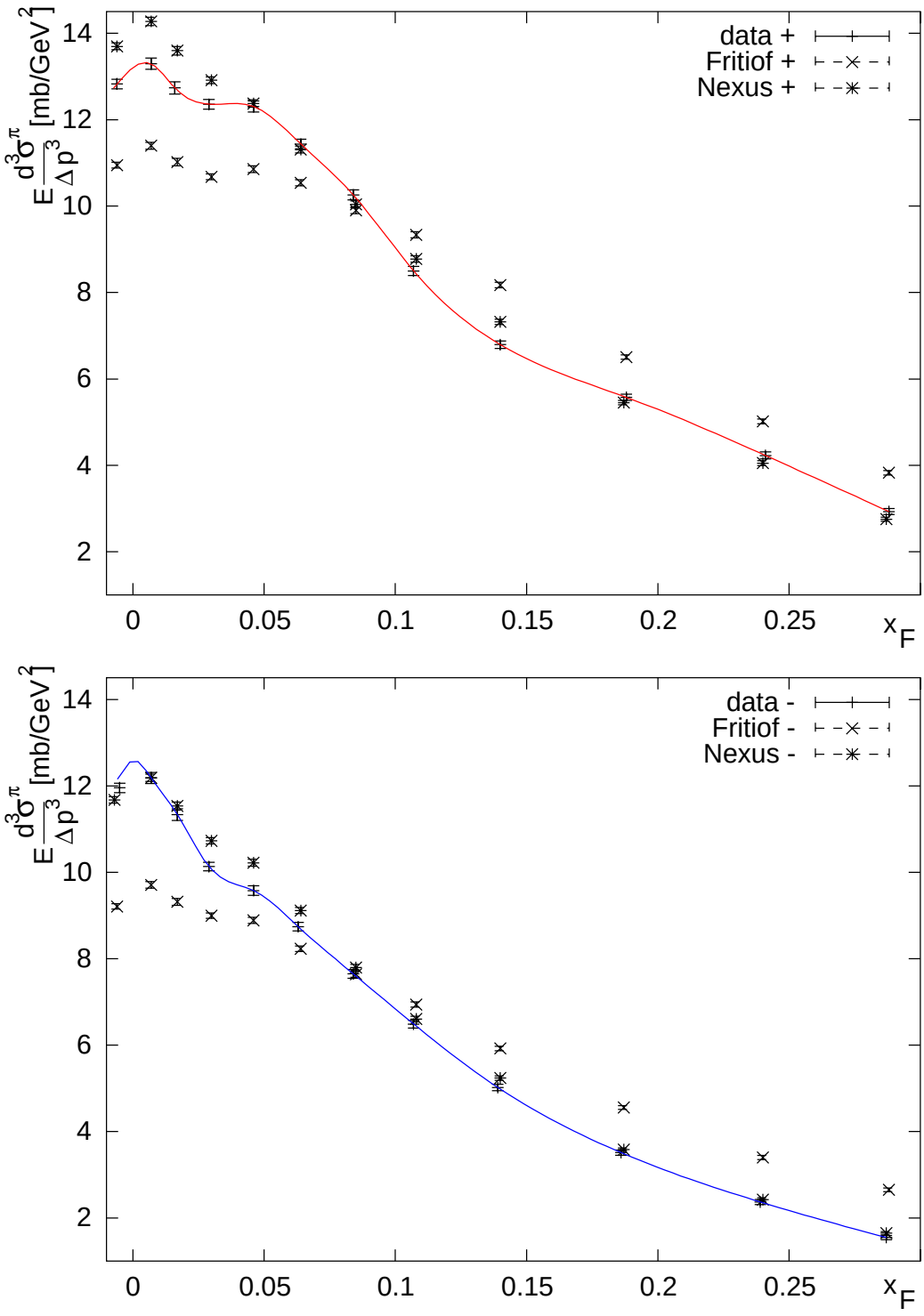

Figure 5.5: Comparison of data with generators Fritiof 7 and Nexus 2 in manually defined bins where $\overline{p_T} = 400\,\mathrm{MeV}$. The line interconnecting the measured points is just to guide the eye.

Fritiof positives		
parameter	value	error
c_1	65.68	41.1
c_2	-2.81	3.5
c_3	-3.19	4.8
c_4	0.19	1.4
c_5	3.56	1.2
N_{bins}	903	
σ_{ASE}	16.9 %	

Fritiof negatives		
parameter	value	error
c_1	55.12	27.8
c_2	-2.93	3.2
c_3	-2.93	4.7
c_4	0.13	1.7
c_5	4.38	1.6
N_{bins}	906	
σ_{ASE}	12.4 %	

Table 5.4: Fit 4.5 parameters of Fritiof7 generated data, binning C

5.4 Experience with corrections

5.4.1 Shifts and σ_{rel}

The effect of a different number of dE/dx fit parameters was tested on manual binning. The results obtained by iterative fitting[1] of all the 12 parameters (ratios of the particle yields, shifts and σ_{rel}s) are considered to be the most reliable ones, because their χ^2 obtained by formula 3.5 is the lowest in all the bins. They are used as reference values ρ^{π}_{12} for the comparison.

For the comparison a relative average deviation is calculated by following formula:

$$\sigma^2_{par} = \frac{1}{N_{bins}} \left(\sum_{i=1}^{N_{bins}} \frac{(\rho^{\pi}_{12} - \rho^{\pi}_{par})^2}{(\rho^{\pi}_{par})^2} \right) \tag{5.1}$$

where $N_{bins} = 13$ is the number of measurements, and ρ^{π}_{par} are the IIC values obtained by compared dE/dx fits.

I have compared the results of the dE/dx fit using a) common shift and σ_{rel} for all the particle species, b) fixed shifts = 0 and fixed $\sigma_{rel} = 1$, c) common shift and fixed $\sigma_{rel} = 1$, d) fixed shifts = 0 and common σ_{rel}. Obtained values of σ_{par} are summarized at the table 5.5 in %.

The data obtained in binnings A – F was evaluated by a dE/dx fit using a common value of the shifts and of theσ_{rel}s, because introduced error is small and the dE/dx fit method is more stable in this case.

Both the shifts and σ_{rel} obtained in different binnings are consistent.

The values of the shifts are typically about 5–10 % of the width of the pion peak. So they are small but not negligible corrections.

[1] All the parameters cannot be fitted all together, as they are correlated. Due to this fact we can fit the parameters by iterative procedure: first fit is performed by common shifts and σ_{rel}s, then the shifts are released and the fit is performed, then the shifts are fixed, σ_{rel}s are released and the fit is performed, ...

charge	a)	b)	c)	d)
positive	1.7	4.4	4.4	2.6
negative	1.9	4.3	4.1	3.4

Table 5.5: Values of σ_{par} for different parameters of dE/dx fit in %

The values of σ_{rel}s are limited within the range $< 0.9; 1.1 >$. Most of the values are below 1, and in about 18 % of bins of the binning C, the value of σ_{rel} is at the lower limit, but only 1.5 % of them is at he upper limit. This could signify overestimation of the dE/dx measurement error.

5.4.2 φ distribution of tracks

The flatness of the φ distributions of tracks is very good within our range of the phase–space. The mean value of χ^2_φ calculated by formula 4.9 is 1.06 for positive tracks and 1.1 for negative ones in the bins of the binning C that were accepted by the interpolation code.

However, in low p_L^{lab} and high p_T bins, the systematic deviations in the φ track distributions are observed, possibly because of the quality of the data – it was realized that the old reconstruction chain produces about 20 % of split tracks in this region, which are rejected by the cut on the number of track points.

Chapter 6

Conclusions

As was shown, interpolation of the measurements by a smooth function 4.3 can only describe the gross features of the inclusive distributions. The fact that it can not describe the details is hidden in high values of σ_{ASE}.

The cleanest result of my effort would be the IIC table which has 882/879 entries for π^+/π^- in the case of optimally chosen binning C. Instead of producing such a table, a Pearl script is provided at:

`http://www.amu.cz/cgi-bin/iic/iic.pl`

This script allows for evaluation of IIC at an arbitrary $[x_F, p_T]$ point using the desired number of the measurements to interpolate. The script then displays a table of the found measurements, evaluated result, and a 3D plot of the measurements, the result, and the interpolation function. The table of found measurements is linked to corresponding `fit.out` files, so one can see the dE/dx fit result for each of the measurements.

If we first define the binning and then look for the cross section values, we have to somehow interpolate. However, interpolation introduces hardly estimated error, so its better to refrain from it.

For this purpose, the method should be reversed: having the $[x_F, p_T]$ point, where we want to evaluate the IIC, we can select some number of surrounding tracks and perform the dE/dx fit using them; thus, avoiding any interpolation.

Preliminary data processed by my method are remarkably consistent with other sources – literature and event generators – so, we can foresee much reliable results applying the method to oncoming data.

Bibliography

[1] NA49 Collaboration: *The NA49 Large Acceptance Hadron Detector*, Nucl. Instrum. Methods Phys. Res. A, 6. 1. 1999

[2] Beiser, F. et al.: *Design and performance of TPC readout electronics for the NA49 experiment*, Nucl. Instrum. Methods Phys. Res. A 385 (1997), 535–546

[3] Bormann, C. et al: *A Software Environment for the NA49 TPCs*, Nucl. Instrum. Methods Phys. Res. A 374 (1996), 227–234

[4] Application Software Group, CN Division, CERN: *DSPACK – Data Manager*, CERN, Geneva 1993

[5] Application Software Group, CN Division, CERN: *MINUIT – Function Minimization and Error Analysis*, CERN, Geneva 1994

[6] Řídký, Jan: *Is There a Hierarchy of the Hadron Low p_T spectra?*, Fortschr. Phys. 36 (1988) 10, 707–780

[7] Slansky, J.: *High-Energy Hadron Production and Inclusive Reactions*, Phys. Letters 11C (1974), 99–188

[8] Horn, D.: *Hadron Physics at Very High Energies*, W. A. Benjamin, Inc., 1973

[9] Collins, P. B. D.: *Hadron Interactions*, Adam Hilger Ltd., 1984

[10] Perl, Martin L.: *High Energy Hadron Physics*, John Wiley & Sons, 1974

[11] Giacomelli, G.: *Inclusive and Semi-inclusive at ISR and Collider Energies*, Int. Journal of Mod. Phys. A, Vol 5, No2 (1990), 223–297

[12] Kafka, T. et al: *One-, two- and three-particle distributions in pp collisions at 205 GeV/c*, Phys. Rev. D 5 (1977) 16, 1261–2193

[13] Bourquin, M., Gaillard, J.-M.: *A Simple Phenomenological Description of Hadron Production*, Nucl. Phys. B 114 (1976), 334–364

[14] Capillupi, P. et al: *Charged Particle Production in Proton-Proton Inclusive Reactions at Very High Energies*, Nucl. Phys. B 79 (1974), 189–258

[15] Alper, B. et al: *Producion Spectra of $\pi^{\pm}$, $K^{\pm}$, $p^{\pm}$, at Large Angles in Proton-Proton Collisions in the CERN Intersecting Storage Rings*, Nucl. Phys. B 100 (1976), 237–290

[16] Blum, W., Rolandi, L.: *Particle Detection with Drift Chambers*, Springler–Verlag Berlin Heidelberg 1993

[17] Leo, W. R.: *Techniques for Nuclear and Particle Physics Experiments*, second edition, Springler–Verlag Berlin Heidelberg

[18] Veres, Gabor: *Status on dE/dx in pp, pPb*, NA49 Collaboration meeting, 8.–13. 3. 1999

[19] Sikler, Ferenc: *Particle identification with global dE/dx*, NA49 Collaboration meeting, 8.–13. 3. 1999

[20] Betev, Latchesar: *'98 p-p data taking*, NA49 Collaboration meeting, 28. 9.–3. 10. 1998, 361–366

[21] Bracinik, Juraj: *The status of inclusive cross section and particle ratios in p-p and p-pPb*, NA49 Collaboration meeting, 28. 9.–3. 10. 1998, 101–118

[22] Bracinik, Juraj: *Calculation of trigger cross section and inclusive cross section for $p + p$*, NA49 preprint, 18. 1. 1999

[23] Rybicki, Andrej: *Study of particle yields using dE/dx fits*, NA49 preprint

[24] Roe, B. P.: *Probability and Statistics in Experimental Physics* Springler–Verlag Berlin Heidelberg 1992

[25] Fischer, H. G.: Talk presented at NA49 workshop in Krakow, 7. 12. 1999

[26] NA49 Collaboration: *NA49 Experimental Results Relevant to the Question of QGP Formation*, Summary of present NA49 results concerning Pb+Pb collisions prepared at the request of the CERN directorate, 23. 11. 1999

[27] Maini, L. et al.: *Special seminar: A new state of matter: Results from the CERN Lead-Beam Programme*, 10. 2. 2000

[28] Pi, H.: *An Event Generator for Interactions Between Hadrons and Nuclei – Fritiof Version 7*, Comput. Phys. Commun. 71 (1992), 173–192

[29] K. Werner: *Strings, Pomerons and the VENUS model of hadronic interactions at ultrarelativistic energies*, Phys. Rep. 232 (1993), 87–299

[30] `http://www-subatech.in2p3.fr/~theo/nexus/`

Appendix A

Kinematic Variables

If we know a particle's three-momentum in laboratory frame $[p_x, p_y, pz = p_L^{lab}]$ and its mass m, we can calculate the particle's CMS longitudal momentum p_L, transverese momentum p_T, Feynman's x_F variable and rapidity y by means of the following formulae ($c \equiv 1$, p_p^{in} is the laboratory momentum of the incomming proton, 158 GeV in our case, m_p is a proton's mass):

$$p_T = \sqrt{p_x^2 + p_y^2} \tag{A.1}$$

$$p_L = \gamma_{CM} \cdot \left(p_L^{lab} - \beta_{CM} \cdot \sqrt{(p_L^{lab})^2 + p_T^2 + m^2} \right) \tag{A.2}$$

$$x_F = \frac{p_L}{p_L^{max}} \tag{A.3}$$

$$y = \frac{1}{2} \ln\left(\frac{E + p_L}{E - p_L} \right) \tag{A.4}$$

where

$$p_L^{max} = \sqrt{\left(\frac{E_{CM}^{in}}{2} \right)^2 - m_p^2} \tag{A.5}$$

$$E = \sqrt{p_L^2 + p_T^2 + m^2} \tag{A.6}$$

$$\beta_{CM} = \frac{p_p^{in}}{E_{tot}^{in}} \tag{A.7}$$

$$\gamma_{CM} = \frac{1}{\sqrt{1 - \beta_{CM}^2}} \tag{A.8}$$

$$E_{tot}^{in} = m_p + \sqrt{p_p^{in} + m_p^2} \tag{A.9}$$

$$E_{CM}^{in} = \sqrt{2\ m_p^2 + m_p \cdot \sqrt{p_p^{in} + m_p^2}} \tag{A.10}$$

Appendix B

Data Measured by NA49

Until the end of the 1999 run period, NA49 had measured different interactions with different energy and detector setup. They can be organized in following data sets:

Table B.1: NA49 data sets

interaction	**year**	**events [K]**	**energy [GeV]**	remark
p-p	1996	410	158	μDST
	1998	250	100	
	1998	150	40	
	1999	800	158	
	1999	110	40	
	1999	200	40	d beam
n-p	1999	200	40	d beam
p-A	1996	550	158/250	μDST
	1999	2000	158	
A-A	96-99	5000	40-160/n	

μDST – data reconstructed to the μDST format, see Appendix C. d beam – the beam used consisted of deuterons extracted from the fragmentation target

For my work I used the only *p-p* data set available in the μDST format, i.e. data from the 1996 run period.

The huge amount of nucleon–nucleon and nucleon–nuclei data recorded in 1999 contains the information from VPP and RCal.

Appendix C

The μDST

C.1 Data Structure

Structure of the μDST file format is clearly explained by its author:

From: Gabor Veres < *Gabor.Veres@cern.ch* >

***** STATISTICS *****

The files have the following amount of events:

p-p:

runs	# of events
1117-1216	407611

p-Pb:

runs	# of evts	filename	reaction	beam E
1744-1755	64375	nppb1.dat	p Pb min. bias	158 GeV
1756-1763	62874	nppb2.dat	p Pb CD$\geq$2	158 GeV
1764-1773	57340	nppb3.dat	p Pb CD$\geq$7	158 GeV
1775-1782	50524	nppb4.dat	pi+ Pb CD$\geq$2	158 GeV
1785-1791	27591	nppb5.dat	pi+ Pb CD$\geq$7	158 GeV
1792-1803	37613	nppb6.dat	p Pb min. bias	158 GeV
1806	2829	nppb7.dat	K+ Pb CD$\geq$1	158 GeV
1811-1829	38816	nppb8.dat	p Al min. bias	158 GeV
1833-1862	68076	nppb9.dat	p Al CD$\geq$1	158 GeV
1868-1871	43789	nppb10.dat	p Pb CD$\geq$2	250 GeV
1881	23548	nppb11.dat	p Pb CD$\geq$7	250 GeV

***** FORMAT, INFORMATION CONTAINED *****

These files contain integer numbers only. That means, that I round every quantity to integer. The format of them is the following:

in case of p-p data:

$<$ *run number*$)$ $-$ 1000 $><$ *event number* $><$ *number of tracks in this event* $>$

in case of p-Pb data:

$<$ $($*run number*$)$ $-$ 1000 $><$ *event number* $><$ *number of tracks in thisevent* $><$ *CD counts* $>$

and in the next N lines (where N = number of tracks) comes the information about the tracks (8 numbers):

$< px >< py >< pz >< charge * dE/dx * 1000 >< (m^2 + w) * 1000 >< flag * (number\ of\ points\ in\ VERTEX\ TPCs) >< flag * (number\ of\ points\ in\ MAIN\ TPC) >< absolute\ sigma\ of\ dE/dx * 1000 >$

The px, py, pz are momentum components at the target, in MeV (!!!). The '$charge$' is the charge of the particle. +1 or -1. '$dedx$' is the truncated mean, which describes the specific ionization. It has 0 value if the calculation of dE/dx was not possible. (It concerns about 5 tracks per million.)

'm^2' is the mass squared coming from the Time Of Flight measurements.

'w' shows the wall which detected the particle:

If the tof detector ID is 32 (Marburg), w=100; 64(Buda) w=200; 128(Dubna) w=300; 256(Buda) w=400

If the track doesn't have TOF information, it has a value of 0. It is very important to regard the 0 as NO INFORMATION, since this is a possible measured value!!! (If 0 was *measured*, I put in a small nonzero value.)

'$numberofpoints$' is the number of clusters found on the track in the Vertex TPS-c and the Main TPC-s.

'$flag$': this is either +1 or -1, depending on the impact parameter of the track, more precisely, on the 'bx' and 'by' distance between the vertex and the track x,y coordinates at the z position of the vertex.

It is -1, if the track is 'far' off:
if((track.bx/2.)**2+(track.by/1.)**2.gt.1.) for p-Pb and if((track.bx/1.5)**2+(track.by/0.5)**2.gt.1.) for p-p. (elliptical cut) Otherwise the flag is +1.

So, if one wants to use this cut, may take the tracks having positive flag only.

For example, I show here the first p-p event:

116 2822 7
333 -237 1565 1304 0 35 0 99
-70 -56 2650 1107 0 37 0 89
227 473 8938 -1236 0 -15 0 148
-147 3 51950 1687 0 0 86 74
-529 131 11009 -1421 0 82 84 45
918 57 35757 1380 0 67 79 50
55 -275 19504 1525 0 68 74 53
and the first p-Pb event: 744 56 6 5

-679 666 2962 1148 0 11 0 166
358 228 1171 3514 0 12 0 278
-332 304 2906 -1224 0 45 0 85
-271 792 8235 -1280 0 -23 0 122
444 -17 33667 -1497 0 0 89 68
228 157 16807 1493 0 69 89 49

C.2 Parameterization of the Bethe-Bloch curve

Along with the *u*DST, appropriate parameterization of the Bethe-Bloch curve is supplied. The shape of BB for different particles is shown on figure 3.1 on page 17. Mentioned parameterization follows as a FORTRAN function. Input parameter is a paticle's $\beta\gamma$.

```
      real*4 function bethe(bg)
      implicit none
c--------------------------------------------------------------------
        real x,x0,x1,b,m,pl,a,bg,d,beta,gamma
        real f,alfa,min,bmin
        alfa=-2.00
        min=3.76
        x0=1.77
        x1=4.
        pl=1.54
c--------------------------------------------------------------------
        bmin=min/sqrt(1.+min*min)
        a=-alfa/2.*(1.-bmin*bmin)/(bmin**(alfa+4.))
        b=min*min*(1.-bmin*bmin*(1.+2./alfa))+log(1.-bmin*bmin)
        m=(x1-x0)/((pl/a-b+1.)/2./log(10.)-x0)
        x=log10(bg)
        d=0
        if(x.gt.x0)then
          d=x-x0+(x0-x1)/m
          if(x.lt.x1)d=d+(x1-x)**m/(m*(x1-x0)**(m-1.))
        endif
        d=d*2.*log(10.)
        beta=bg/sqrt(1.+bg*bg)
        gamma=bg/beta
        f=a*(beta**alfa)*(b+2.*log(gamma)-beta*beta-d)
        f=f*(1.+0.1800*log(f)-0.0155*log(f)*log(f))
      bethe = f
      end
```

Appendix D

Source Codes of Mentioned Programmes

Table of Content

binme.C.....sheets 60 to 62 (3) pages 119-123 243 lines
phase_fit.f.....sheets 62 to 62 (1) pages 124-124 12 lines
ph_fcn.f.....sheets 63 to 64 (2) pages 125-127 147 lines
read_and_cut.f.....sheets 64 to 67 (4) pages 128-133 330 lines
minfit.f.....sheets 67 to 67 (1) pages 134-134 34 lines
fcn.f.....sheets 68 to 72 (5) pages 135-143 487 lines
cross.f.....sheets 72 to 73 (2) pages 144-146 169 lines
intfit.f.....sheets 74 to 74 (1) pages 147-147 15 lines
int_ic.f.....sheets 74 to 76 (3) pages 148-151 202 lines
table_ic.f.....sheets 76 to 78 (3) pages 152-155 187 lines
tell_me_iic.f.....sheets 78 to 80 (3) pages 156-159 212 lines
statbins.f.....sheets 80 to 84 (5) pages 160-167 430 lines
generators_ic.f.....sheets 84 to 87 (4) pages 168-173 334 lines
incl_pp.f.....sheets 87 to 93 (7) pages 174-185 643 lines

The listed programme codes are aviable at the following URL:

`http://www.amu.cz/iic/iic.src.tgz`